

Spatial hierarchical modeling of threshold exceedances using rate mixtures

Rishikesh Yadav¹  | Raphaël Huser¹  | Thomas Opitz² 

¹Computer, Electrical and Mathematical Sciences and Engineering (CEMSE) Division, King Abdullah University of Science and Technology (KAUST), Thuwal, Saudi Arabia

²INRAE, UR546 Biostatistics and Spatial Processes, Avignon, France

Correspondence

Raphaël Huser, Computer, Electrical and Mathematical Sciences and Engineering (CEMSE) Division, King Abdullah University of Science and Technology (KAUST), Thuwal 23955-6900, Saudi Arabia.

Email: raphael.huser@kaust.edu.sa

Funding information

King Abdullah University of Science and Technology (KAUST) Office of Sponsored Research (OSR), Grant/Award Number: OSR-CRG2017-3434

Abstract

We develop new flexible univariate models for light-tailed and heavy-tailed data, which extend a hierarchical representation of the generalized Pareto (GP) limit for threshold exceedances. These models can accommodate departure from asymptotic threshold stability in finite samples while keeping the asymptotic GP distribution as a special (or boundary) case and can capture the tails and the bulk jointly without losing much flexibility. Spatial dependence is modeled through a latent process, while the data are assumed to be conditionally independent. Focusing on a gamma–gamma model construction, we design penalized complexity priors for crucial model parameters, shrinking our proposed spatial Bayesian hierarchical model toward a simpler reference whose marginal distributions are GP with moderately heavy tails. Our model can be fitted in fairly high dimensions using Markov chain Monte Carlo by exploiting the Metropolis-adjusted Langevin algorithm (MALA), which guarantees fast convergence of Markov chains with efficient block proposals for the latent variables. We also develop an adaptive scheme to calibrate the MALA tuning parameters. Moreover, our model avoids the expensive numerical evaluations of multifold integrals in censored likelihood expressions. We demonstrate our new methodology by simulation and application to a dataset of extreme rainfall events that occurred in Germany. Our fitted gamma–gamma model provides a satisfactory performance and can be successfully used to predict rainfall extremes at unobserved locations.

KEY WORDS

Bayesian hierarchical modeling, extended generalized Pareto distribution, extreme event, Markov chain Monte Carlo, penalized complexity prior, precipitation extremes

1 | INTRODUCTION

Atmospheric, meteorologic, hydrologic, and land surface processes among others are prone to extreme episodes, which are believed to increase in frequency and severity in the context of a changing climate and global warming (see, e.g., Arneth et al., 2019; Power & Delage, 2019; Witze, 2018). To quantify environmental risk, for example, associated with weather variables (Davison & Gholamrezaee, 2012; de Fondeville & Davison, 2018; Huser & Davison, 2014) or air pollution (Eastoe & Tawn, 2009; Vettori et al., 2019, 2020), or to attribute certain extreme events to human influence (Risser &

Wehner, 2017), it is crucial to model and predict the univariate behavior of extreme events, while accounting for spatial dependence. Extreme-value theory (EVT) provides a natural methodological framework to tackle this problem; for more details, see, for example, the review papers Davison et al. (2012), Davison and Huser (2015), Davison et al. (2019), and Huser and Wadsworth (2020).

In this article, we first study a hierarchical construction that leads to new univariate tail models, which extend the classical EVT approach by gaining flexibility at finite levels. We then exploit this hierarchical construction in a Bayesian framework for the modeling of spatial extremes by embedding a latent process with spatial dependence, while keeping the desired unconditional marginal distributions.

Under mild conditions, classical univariate EVT suggests using the generalized Pareto (GP) distribution for modeling extreme events defined as high threshold exceedances (Davison & Smith, 1990). More precisely, let Y be a random variable following a distribution F with finite or infinite upper endpoint $y_F = \sup\{y \in \mathbb{R} : F(y) < 1\}$. Then, for a wide class of distributions F , high threshold exceedances $(Y - u) | Y > u$ may be *asymptotically* approximated as

$$\Pr(Y - u \leq y | Y > u) = \frac{F(u + y) - F(u)}{1 - F(u)} \approx H_{\tau, \xi}(y) = 1 - (1 + \xi y / \tau)^{-1/\xi}, \quad (1)$$

as the threshold u converges to y_F , where $H_{\tau, \xi}(y)$ denotes the GP distribution function with scale parameter $\tau > 0$ and shape parameter $\xi \in \mathbb{R}$ (also called the tail index), defined over $\{y > 0 : 1 + \xi y / \tau > 0\}$. In other words, $1 - F(y) \approx \zeta_u \{1 - H_{\tau, \xi}(y - u)\}$, for $y > u$ large, where $\zeta_u = \Pr(Y > u)$. When $\xi = 0$, the distribution (1) is interpreted as the limit $\xi \rightarrow 0$, and we obtain the exponential distribution function $H_{\tau, 0}(y) = 1 - \exp(-y/\tau)$, $y > 0$. When $\xi < 0$, the support is bounded, whereas when $\xi \geq 0$, it is unbounded. Short, light, and heavy tails correspond to $\xi < 0$, $\xi = 0$, and $\xi > 0$, respectively, with ξ controlling the tail weight.

In practice, the choice of a good threshold u should reflect the transition around which the asymptotic regime takes place for the tail approximation (1) to be valid. This implies a bias-variance trade-off, as a high threshold u leads to a good approximation (low bias) but yields a small number of exceedances (high variance), and vice versa for a low threshold. Experience shows that automatic threshold selection procedures are not always reliable. It is often difficult to find a good, natural, and interpretable threshold, and parameter estimates are often sensitive to this choice (Scarrott & MacDonal, 2012). This has motivated the development of *subasymptotic* models for extremes, which are more flexible than the asymptotic GP distribution at finite levels, while keeping a GP-like behavior in the tail; see, for example, Frigessi et al. (2003), Carreau and Bengio (2009), and Papastathopoulos and Tawn (2013), among others; see Scarrott and MacDonal (2012) for a review of models describing jointly the bulk and the tail of the distribution. With subasymptotic tail models, parameter estimates are usually less sensitive to the threshold, the choice of which then becomes less crucial for inference, and we can thus set lower thresholds. In some approaches (see, e.g., Naveau et al., 2016; Stein, 2020a, 2020b), the threshold choice is even bypassed by adding parameters that provide separate control over bulk properties of the distribution, such that models are expected to provide a satisfactory fit of the tail, even if the whole sample is used for estimation.

In this article, we propose a novel Bayesian hierarchical modeling framework for subasymptotic threshold exceedances. It has an intuitive interpretation, permits fully Bayesian inference, and can naturally incorporate covariate information and be extended to the spatial setting. Several Bayesian hierarchical models were already proposed in the literature to model threshold exceedances; see, for example, Cooley et al. (2007), Opitz et al. (2018), and Castro-Camilo et al. (2019). However, unlike the latent Gaussian models proposed therein, our construction makes sure that the unconditional distribution (obtained after integrating out latent random effects) remains of the desired form, with the GP distribution as a particular case. Precisely, we extend the characterization of the GP distribution as an exponential mixture with rate parameter following a gamma distribution. Let $\text{Exp}(\lambda)$ denote the exponential distribution with rate $\lambda > 0$, $\text{Gamma}(\alpha, \beta)$ denote the gamma distribution with rate $\alpha > 0$ and shape $\beta > 0$, that is, with density $g(y) = \{\Gamma(\beta)\}^{-1} \alpha^\beta y^{\beta-1} \exp(-\alpha y)$, $y > 0$, and $\text{GP}(\tau, \xi)$ denote the GP distribution with scale $\tau > 0$ and shape ξ as defined in (1). Then we have

$$\left. \begin{array}{ll} Y | \Lambda & \sim \text{Exp}(\Lambda) \\ \Lambda & \sim \text{Gamma}(\alpha, \beta) \end{array} \right\} \Rightarrow Y \sim \text{GP}(\alpha/\beta, 1/\beta); \quad (2)$$

see Reiss and Thomas (2007), Bortot and Gaetan (2014, 2016), Bopp and Shaby (2017), and Bacro et al. (2020). In other words, exponentially decaying tails become heavier by making their rate parameter Λ random. By integrating out the

latent variable Λ in the hierarchical construction in (2), we obtain the GP distribution for the data Y . Our new tail models (detailed further in Section 2) are constructed as in (2), but we modify the top and/or lower levels of the hierarchy in order to gain in flexibility, while keeping the GP distribution with $\xi \geq 0$ as a special or boundary case. Moreover, we penalize departure from the GP distribution in the Bayesian framework by specifying penalized complexity (PC) priors (Simpson et al., 2017) designed to shrink complex models toward simpler counterparts, thus preventing overfitting. This avoids estimating unreasonable tail models, and guarantees that the fitted distribution will not be too far away from the GP distribution which is supported by asymptotic theory, unless the data provide strong evidence that a different subasymptotic behavior prevails. In other words, our proposed models are constrained to remain in the “neighborhood” of moderately heavy-tailed GP distributions. Our modeling approach based on extensions of (2) is general and can potentially generate a wide variety of new models with light and heavy tails and various behaviors in the bulk. Below, we mainly focus on a parsimonious extension of (2), which assumes a gamma distribution in both levels of the hierarchy, although we also discuss other possible models with interesting tail properties.

For spatial modeling, we incorporate spatial dependence at the latent level, while assuming that the data are conditionally independent given the latent process. Specifically, we assume that the observed spatial process $Y(\mathbf{s})$, $\mathbf{s} \in S \subset \mathbb{R}^2$, may be described analogously to (2) with a hierarchical representation in terms of a latent spatially structured process $\Lambda(\mathbf{s})$, such that the data $Y(\mathbf{s}_1)$ and $Y(\mathbf{s}_2)$ at any two distinct locations $\mathbf{s}_1, \mathbf{s}_2 \in S$, $\mathbf{s}_1 \neq \mathbf{s}_2$, are independent given $\Lambda(\mathbf{s}_1)$ and $\Lambda(\mathbf{s}_2)$. This conditional independence assumption is common in Bayesian hierarchical models (Banerjee et al., 2014; Cooley et al., 2007; Opitz et al., 2018) and is, to some extent, akin to using a “nugget effect” in classical geostatistics (Cressie, 1993), which captures measurement errors or unstructured local variations in the data. Here, we make this assumption mainly to keep the model simple and identifiable, and for computational convenience in order to efficiently handle the censoring of nonextreme values in our inference procedure. More precisely, to fit our models to threshold excesses $Y(\mathbf{s}) > u(\mathbf{s})$ for some moderately high threshold $u(\mathbf{s})$, we design a generic Markov chain Monte Carlo (MCMC) sampler that efficiently exploits the hierarchical representation. Low values such that $Y(\mathbf{s}) \leq u(\mathbf{s})$ are treated as censored and imputed by simulation in our MCMC algorithm. Thanks to the conditional independence assumption, multivariate censoring can be conveniently reduced to univariate site-by-site imputations. This computational benefit is significant, and it contrasts with the high computational burden due to multivariate censoring in peaks-over-threshold inference for most spatial extremes models (Castro-Camilo & Huser, 2020; Huser et al., 2017; Huser & Wadsworth, 2019; Wadsworth & Tawn, 2014). This approach allows us to tackle higher spatial dimensions more easily. Furthermore, to efficiently sample from the posterior distribution and accelerate the mixing of MCMC chains, we update the large number of latent parameters jointly (in one block) based on the Metropolis-adjusted Langevin algorithm (MALA, see Roberts & Tweedie, 1996 and Roberts & Rosenthal, 1998) and we adaptively calibrate the MALA tuning parameters to obtain suitable acceptance rates. Our fully Bayesian algorithm can easily handle missing values and be used for prediction at unobserved locations. Finally, in spite of the conditional independence assumption, nontrivial extremal dependence structures may be obtained by carefully specifying the dependence structure of the latent process $\Lambda(\mathbf{s})$. This contrasts with classical latent Gaussian models for extremes (e.g., Cooley et al., 2007; Opitz et al., 2018), which are unable to capture strong extremal dependence.

The article is organized as follows. In Section 2, we define our hierarchical construction of univariate distributions and characterize their tail behavior. Spatial hierarchical modeling is developed in Section 3, and we describe Bayesian inference and our MCMC implementation using latent variables in Section 4. An extensive simulation study is reported in Section 5 showing that our approach works well in various scenarios. We use our approach based on a gamma–gamma hierarchical model to study extreme events in daily precipitation measurements recorded at 150 sites in Germany in Section 6. Concluding remarks are given in Section 7.

2 | HIERARCHICAL MODELS FOR THRESHOLD EXCEEDANCES

2.1 | Univariate tail properties in rate mixture constructions

For flexible subasymptotic tail modeling, we seek to replace the distributions in the hierarchical representation (2) of the GP distribution by more general parametric families that contain the exponential–gamma mixture considered by Bopp and Shaby (2017) as a special (or boundary) case.

Specifically, we construct new rate mixture models for the data $Y \sim F$ as follows. We consider a family of distributions $F_{Y|\Lambda=\lambda}(\cdot)$ with rate parameter λ and supported in $[0, +\infty)$, where $\Lambda \geq 0$ is a latent random variable, such that $Y|\Lambda \sim F_{Y|\Lambda}(\cdot)$. Equivalently, we have the following ratio representation, which is useful for simulation and inference:

$$Y|\Lambda \stackrel{D}{=} \frac{\tilde{Y}}{\Lambda}, \quad \text{with} \quad \Lambda \geq 0 \perp\!\!\!\perp \tilde{Y} \geq 0, \quad \tilde{Y} \sim F_{Y|\Lambda=1}(\cdot), \quad (3)$$

where “ $\stackrel{D}{=}$ ” means equality in distribution and $\perp\!\!\!\perp$ denotes the independence of random variables. The (unconditional) upper tail behavior of Y is determined by the interplay between the upper tail of \tilde{Y} and the lower tail of Λ (i.e., the upper tail of $1/\Lambda$). We now shortly discuss two general and particularly interesting scenarios. Recall that a positive function $r(\cdot)$ is regularly varying at infinity with index $a \in \mathbb{R}$ if $r(tx)/r(t) \rightarrow x^a$ as $t \rightarrow \infty$ and $x > 0$; when $a = 0$, $r(\cdot)$ is slowly varying at infinity.

In the first scenario, we assume that $1/\Lambda$ in (3) has power-law tail decay, that is, its distribution is regularly varying with index $-a < 0$, such that $\Pr(1/\Lambda > y) = r_0(y)y^{-a}$, $y > 0$, and $r_0(\cdot) > 0$ is a slowly varying function. If the distribution $F_{Y|\Lambda=1}(\cdot)$ in (3) has a lighter upper tail than that of $1/\Lambda$, such that $\mathbb{E}(\tilde{Y}^{a+\varepsilon}) < \infty$ for some $\varepsilon > 0$ with $\tilde{Y} \sim F_{Y|\Lambda=1}(\cdot)$, then Breiman's lemma (Breiman, 1965) implies that

$$1 - F(y) = \Pr(Y > y) \sim \mathbb{E}(\tilde{Y}^a) \Pr(1/\Lambda > y), \quad y \rightarrow \infty. \quad (4)$$

Therefore, the heavier-tailed random factor $1/\Lambda$ in (3) dominates the tail behavior of Y in this case, while the lighter-tailed random factor \tilde{Y} contributes to extreme survival probabilities only through a scaling factor.

In the second scenario, we assume that both \tilde{Y} and $1/\Lambda$ in (3) have tails of Weibull type, which are lighter than power-law tails. Formally, we assume that there exist regularly varying functions \tilde{r}, r_Λ (with any index of regular variation), rate parameters $\tilde{\alpha}, \alpha_\Lambda > 0$ and shape parameters (also referred to as Weibull indexes) $\tilde{\eta}, \eta_\Lambda > 0$ such that

$$\Pr(\tilde{Y} > y) = \tilde{r}(y) \exp(-\tilde{\alpha}y^{\tilde{\eta}}), \quad \Pr(1/\Lambda > y) = r_\Lambda(y) \exp(-\alpha_\Lambda y^{\eta_\Lambda}). \quad (5)$$

Then, the variable Y constructed as in (3) also has a tail of Weibull type, with representation $\Pr(Y > y) = r_Y(y) \exp(-\alpha_Y y^{\eta_Y})$ similarly to (5). Its Weibull index is $\eta_Y = (\tilde{\eta}\eta_\Lambda)/(\tilde{\eta} + \eta_\Lambda) < \min(\tilde{\eta}, \eta_\Lambda)$, such that the tail of Y always has a slower decay rate than that of each random factor \tilde{Y} and $1/\Lambda$, while its rate parameter α_Y is given by

$$\alpha_Y = \tilde{\alpha}^{1-b} \alpha_\Lambda^b \left\{ \left(\frac{\alpha_\Lambda}{\tilde{\alpha}} \right)^b + \left(\frac{\tilde{\alpha}}{\alpha_\Lambda} \right)^{1-b} \right\}, \quad b = \frac{\tilde{\eta}}{\tilde{\eta} + \eta_\Lambda};$$

see Arendarczyk and Debicki (2011). In the following sections, we exploit the rate mixture construction (3) and we propose new subasymptotic univariate tail models. In Section 2.2, our proposed model is heavy-tailed with the GP distribution as a special case and we focus on it for spatial modeling in Sections 3–6, while in Section 2.3, our proposed construction is a flexible model of Weibull type and has the GP distribution as a limiting boundary case.

2.2 | Gamma-gamma model

Replacing the exponential distribution of $F_{Y|\Lambda}(\cdot)$ in (2) by a gamma distribution yields the hierarchical gamma-gamma model, which may be written as

$$Y|\Lambda \sim \text{Gamma}(\Lambda, \beta_1), \quad \Lambda \sim \text{Gamma}(\alpha, \beta_2), \quad \alpha, \beta_1, \beta_2 > 0; \quad (6)$$

that is, $F_{Y|\Lambda=\lambda}(\cdot)$ is the $\text{Gamma}(\lambda, \beta_1)$ distribution. The model (6) simplifies to the GP distribution obtained in (2) when $\beta_1 = 1$. The distribution of Y corresponds to a rescaled F_{v_1, v_2} distribution with degrees of freedom $v_1 = 2\beta_1$ and $v_2 = 2\beta_2$, and scaling factor $\alpha\beta_1/\beta_2$, such that $Y \stackrel{D}{=} (\alpha\beta_1/\beta_2)Z$, with $Z \sim F_{2\beta_1, 2\beta_2}$. Its density is

$$f(y) = \alpha^{-\beta_1} \frac{\Gamma(\beta_1 + \beta_2)}{\Gamma(\beta_1)\Gamma(\beta_2)} \left(1 + \frac{y}{\alpha}\right)^{-(\beta_1 + \beta_2)} y^{\beta_1-1}, \quad y > 0. \quad (7)$$

The r th moment of Y is finite whenever $\beta_2 > r$, and is given as

$$\mathbb{E}(Y^r) = \frac{\alpha^r \Gamma(\beta_1 + \beta_2) \Gamma(\beta_1 + r) \Gamma(\beta_2 - r)}{\Gamma(\beta_2) \Gamma(\beta_1) \Gamma(\beta_1 + \beta_2 + 2)}, \quad \beta_2 > r.$$

From (4), or directly from (7), we deduce that the gamma–gamma model has a heavy power-law tail. The tail index of the limiting GP distribution (1) is equal to $\xi = 1/\beta_2$, and hence β_2 determines the tail decay rate of the distribution function F of Y . Further details are provided in the Supplementary Material.

2.3 | Model extension with Weibull-type tail behavior

The gamma–gamma model (6) yields heavy tails (i.e., with a positive tail index, $\xi > 0$) and thus has a relatively slow power-law tail decay. For data with a light upper tail (i.e., with a tail index equal to zero, $\xi = 0$), we now discuss a flexible model extension based on the hierarchical construction (3), which provides a faster tail decay than the gamma–gamma model, while keeping the heavy-tailed GP distribution on the boundary of the parameter space. Specifically, we propose the following hierarchical model:

$$\begin{aligned} Y^{1/k}|\Lambda &\sim \text{Gamma}(\Lambda, \beta_1), \quad k, \beta_1 > 0, \\ \Lambda &\sim \text{GIG}(\alpha/2, b, \beta_2), \quad (\alpha, b, \beta_2) \in D_{\text{GIG}}, \end{aligned} \quad (8)$$

where the latent rate parameter Λ is assumed to follow the generalized inverse Gaussian (GIG) distribution with parameters $\alpha/2$, b , and β_2 , and where D_{GIG} denotes its parameter space. More precisely, the $\text{GIG}(\alpha, b, \beta)$ density is $g(y) = (a/b)^{\beta/2} \{2K_\beta(\sqrt{ab})\}^{-1} y^{\beta-1} \exp\{-(ay + b/y)/2\}$, $a \geq 0$, $b \geq 0$, $y > 0$, with parameter constraints on β given by $-\infty < \beta < \infty$ if $a, b > 0$, by $\beta > 0$ if $b = 0$ and $a > 0$, and by $\beta < 0$ if $a = 0$ and $b \geq 0$, and where K_β denotes the modified Bessel function of second kind with parameter β . The GIG distribution has an exponentially decaying tail (i.e., Weibull-type tail with Weibull index one).

Model (8) can also be represented as the ratio $Y = (\tilde{Y}/\Lambda)^k$ with $\tilde{Y} \sim \text{Gamma}(1, \beta_1)$ independent of $\Lambda \sim \text{GIG}(\alpha/2, b, \beta_2)$. This model generalizes the gamma–gamma construction in (6), which is on the boundary of the parameter space with $b = 0$, $k = 1$, and $\beta_2 > 0$. Hence, the model captures a wide range of tail behaviors, from very light tails to relatively heavy tails. Specifically, when $b > 0$, the random variables \tilde{Y}^k and $1/\Lambda^k$ have Weibull-type tails, with Weibull indexes both equal to $1/k$. From (5), we deduce that Y has Weibull index $\eta_Y = (1/k^2)/(2/k) = 1/(2k) > 0$. Thus, when $b > 0$, this model can capture any Weibull tail with any Weibull index, while when $b = 0$, it can capture any power-law tail with any positive tail index $k/\beta_2 > 0$, thanks to Breiman's lemma (4).

3 | A BAYESIAN SPATIAL GAMMA–GAMMA MODEL

3.1 | Bayesian hierarchical modeling framework

Accounting for spatial dependence is important for a variety of reasons, even if the precise estimation of the extremal dependence structure is of secondary importance. First, this allows to borrow strength across locations to reduce the uncertainty and improve the estimation of marginal distributions and of high quantiles. Second, a proper spatial model is needed whenever prediction at unobserved locations is required.

Let $Y(\mathbf{s})$, $\mathbf{s} \in S \subset \mathbb{R}^2$, be the spatial process of interest, and assume that we observe it at a finite set of locations $s_1, \dots, s_d \in S$. There are different approaches to model the dependence structure of $\mathbf{Y} = (Y_1, \dots, Y_d)^T$, where $Y_j = Y(s_j) \sim F_{Y_j}$. One possibility is to directly bind together the marginals of Y_1, \dots, Y_d through a *copula* model (i.e., a multivariate distribution with standard uniform margins) without assuming any hierarchical structure; we call this the *copula approach*. Let C_Y denote the underlying copula of the data \mathbf{Y} , which is unique if \mathbf{Y} has a continuous distribution. Then \mathbf{Y} has distribution function $F(y_1, \dots, y_d) = C_Y\{F_{Y_1}(y_1), \dots, F_{Y_d}(y_d)\}$ and density $f(y_1, \dots, y_d) = c_Y\{F_{Y_1}(y_1), \dots, F_{Y_d}(y_d)\} \prod_{j=1}^d f_{Y_j}(y_j)$, if it exists, where c_Y is the copula density and f_{Y_1}, \dots, f_{Y_d} are the marginal densities. To model threshold exceedances with respect to a fixed threshold vector $\mathbf{u} = (u_1, \dots, u_d)^T$, it is common to censor observations Y_j falling below a corresponding threshold u_j . In the copula approach, the likelihood contribution of an observation $\mathbf{y} = (y_1, \dots, y_d)^T$ such that $y_j \geq u_j$, $j = 1, \dots, j_0$, and $y_j < u_j$, $j = j_0 + 1, \dots, d$, is

$$\frac{\partial^{j_0}}{\partial y_1 \dots \partial y_{j_0}} F(\mathbf{y}) \Big|_{y_{j_0+1}=u_{j_0+1}, \dots, y_d=u_d} = \int_{-\infty}^{u_{j_0+1}} \dots \int_{-\infty}^{u_d} f(y_1, \dots, y_d) dy_{j_0+1} \dots dy_d. \quad (9)$$

When $j_0 < d$, multivariate distribution functions must be calculated to evaluate (9). For many copula models (e.g., Gaussian, Student's t), this requires expensive multivariate numerical integrations. Then, the computational cost can become prohibitively high if the dimension d is large, and accuracy issues may arise.

Here, we instead use the hierarchical approach, where the process $Y(\mathbf{s})$ is assumed to be conditionally independent given a latent process $\Lambda(\mathbf{s})$ with spatial dependence. Let $\Lambda_j = \Lambda(\mathbf{s}_j)$, $j = 1, \dots, d$, and $\Lambda = (\Lambda_1, \dots, \Lambda_d)^T$. We assume that, conditional on Λ , an observation Y_j is independent of the other observations $Y_{j'}, j' \neq j$. The vector of latent variables Λ , on the other hand, is specified through a copula C_Λ . This *hierarchical approach* with a *latent copula* separates the observed process \mathbf{Y} from the latent variables Λ . Note that in the Bayesian modeling literature, latent variables are often used to capture spatiotemporal patterns in marginal distributions (e.g., spatiotemporal trends), while here the latent process $\Lambda(\mathbf{s})$ is part of the model formulation to ensure the required *unconditional* marginal distributions (e.g., of gamma-gamma type as in (6)) and to capture spatial dependence. In particular, this implies that the latent variables involved in different replicates of the process $Y(\mathbf{s})$ will also be different. Moreover, although the conditional independence assumption may be seen as a restriction, it still permits to capture a wide range of dependence structures (see Section 3.4), and it has significant computational benefits. By augmenting the data \mathbf{Y} with the latent variables Λ , the censored likelihood (9) can be formulated in terms of univariate censored terms for the conditionally independent components $Y_j|\Lambda_j$, while no censoring is required for Λ . In Section 4.2, we exploit this latent variable approach for fully Bayesian inference using Markov chain Monte Carlo (MCMC).

We now describe our proposed Bayesian spatial modeling framework in more detail. Let $\Theta = (\Theta_Y^T, \Theta_\Lambda^{\text{mar}^T}, \Theta_\Lambda^{\text{cop}^T})^T$ be the vector of unknown hyperparameters, where Θ_Y controls the conditional distribution of observations, and $\Theta_\Lambda = (\Theta_\Lambda^{\text{mar}^T}, \Theta_\Lambda^{\text{dep}^T})^T$ contains parameters for the latent process $\Lambda(\mathbf{s})$, with $\Theta_\Lambda^{\text{mar}}$ controlling marginal distributions and $\Theta_\Lambda^{\text{dep}}$ controlling the dependence structure. Our general spatial hierarchical construction is specified as

$$\begin{aligned} Y_j|\Lambda, \Theta_Y &\stackrel{\text{ind}}{\sim} F_{Y|\Lambda_j}(\cdot; \Theta_Y), \quad j = 1, \dots, d, \\ \Lambda|\Theta_\Lambda &\sim C_\Lambda\{F_{\Lambda_1}(\cdot; \Theta_\Lambda^{\text{mar}}), \dots, F_{\Lambda_d}(\cdot; \Theta_\Lambda^{\text{mar}}); \Theta_\Lambda^{\text{dep}}\}, \\ \Theta &\sim \pi(\Theta), \end{aligned} \tag{10}$$

where C_Λ refers to the spatial copula of Λ , $F_{\Lambda_j}(\cdot; \Theta_\Lambda^{\text{mar}})$ denotes the marginal distribution of Λ_j , $j = 1, \dots, d$, and $\pi(\Theta)$ is the prior distribution of the parameter vector Θ . The joint distribution of \mathbf{Y} , Λ , and Θ can be decomposed into conditional distributions as $\pi(\mathbf{Y}, \Lambda, \Theta_Y, \Theta_\Lambda) = \pi(\mathbf{Y}|\Lambda, \Theta_Y) \pi(\Lambda|\Theta_\Lambda) \pi(\Theta)$, where $\pi(\cdot)$ denotes a generic (conditional) distribution. The joint posterior distribution $\pi(\Lambda, \Theta|\mathbf{Y})$ of latent variables Λ and hyperparameters Θ is then proportional to $\pi(\mathbf{Y}, \Lambda, \Theta)$, and the posterior distribution of hyperparameters Θ is obtained by integrating out the latent parameters Λ , that is,

$$\pi(\Theta|\mathbf{Y}) = \int \pi(\Lambda, \Theta|\mathbf{Y}) d\Lambda. \tag{11}$$

The dimension of the integration domain in (11) can be very high if there are a lot of latent variables. We solve this issue in Section 4 by implementing an MCMC algorithm, in which the latent variables Λ are imputed and updated at each iteration.

3.2 | A spatial gamma-gamma model

We now present a specific Bayesian hierarchical model of the form (10) that is based on the gamma-gamma construction (6) with a latent Gaussian copula process for the spatial dependence in Λ . Here, $\Theta_Y = \beta_1 > 0$, $\Theta_\Lambda^{\text{dep}}$ contains the correlation parameters of the latent process $\Lambda(\mathbf{s})$, and $\Theta_\Lambda^{\text{mar}} = (\alpha, \beta_2)^T \in (0, \infty)^2$. We focus here on the isotropic exponential correlation function $\sigma(h) = \exp(-h/\rho)$, $h \geq 0$, with range $\rho > 0$, so that $\Theta_\Lambda^{\text{dep}} = \rho$, although other correlation functions are also possible. We write Φ for the univariate standard normal distribution and Φ_ρ for the zero mean and unit variance multivariate normal distribution associated to any collection of d sites $\mathbf{s}_1, \dots, \mathbf{s}_d$, and parametrized by the correlation matrix $\Sigma(\rho)$ with entries $\Sigma_{i_1 i_2} = \sigma(\|\mathbf{s}_{i_1} - \mathbf{s}_{i_2}\|) = \exp(-\|\mathbf{s}_{i_2} - \mathbf{s}_{i_1}\|/\rho)$, $1 \leq i_1, i_2 \leq d$. The $\text{Gamma}(\alpha, \beta)$ distribution function is denoted by $\Gamma(\cdot; \alpha, \beta)$. Following (10), we define the gamma-gamma hierarchical model with latent Gaussian copula as

$$\begin{aligned} Y_j|\Lambda, \Theta_Y &\stackrel{\text{ind}}{\sim} \Gamma(\cdot; \Lambda_j, \beta_1), \quad j = 1, \dots, d, \\ \Lambda|\Theta_\Lambda &\sim \Phi_\rho^{-1}\{\Gamma(\cdot; \alpha, \beta_2)\}, \dots, \Phi_\rho^{-1}\{\Gamma(\cdot; \alpha, \beta_2)\}], \\ \Theta &\sim \pi(\Theta) = \pi(\alpha) \times \pi(\beta_1) \times \pi(\beta_2) \times \pi(\rho). \end{aligned} \quad (12)$$

While a Gaussian copula is specified in (12), other copula models with stronger tail dependence (e.g., the elliptically symmetric Student's t copula with $v > 0$ degrees of freedom and dispersion matrix $\Sigma(\rho)$) are also possible. The implied extremal dependence structure is discussed in Section 3.4. Covariate information may be included in various ways into the model parameters. Here, because α describes the scale of the marginal distribution of the process $Y(s)$, a natural approach is to use a log-linear specification of the form $\log \alpha = \log \alpha_0 + \alpha_1 x_1 + \dots + \alpha_p x_p$ for some known covariates x_1, \dots, x_p . Similarly, we may add covariate information in the parameter β_2 as $\log \beta_2 = \log \beta_{2;0} + \beta_{2;1} z_1 + \dots + \beta_{2;q} z_q$, where z_1, \dots, z_q are (potentially different) covariates. We next describe our choice of prior distributions for the hyperparameters of the gamma–gamma model (12).

3.3 | Prior distributions for hyperparameters

Appropriate prior distributions in the model (12) need to be designed for the components of the hyperparameter vector Θ , and special care is required for the shape parameters β_1 and β_2 , which represent the “distance” to the GP model and the upper tail decay rate, respectively. A possible choice is to select an informative prior distribution $\pi(\beta_1)$ for $\beta_1 > 0$ that shrinks our mixture model (6) toward the GP with $\beta_1 = 1$, believed to be valid in the limit. This can be achieved through the concept of penalized-complexity (PC) priors (Simpson et al., 2017). PC priors assume a constant-rate exponential distribution for the square root of the Kullback–Leibler divergence with respect to a simpler reference model. Let $\gamma(\cdot; \lambda, \beta_1)$ be the Gamma(λ, β_1) density and $\gamma(\cdot; \lambda, 1)$ be the Exp(λ) density. The (asymmetric) Kullback–Leibler divergence of $\gamma(\cdot; \lambda, \beta_1)$ with respect to $\gamma(\cdot; \lambda, 1)$ is

$$\begin{aligned} \text{KLD}\{\gamma(\cdot; \lambda, \beta_1) \parallel \gamma(\cdot; \lambda, 1)\} &= \int_0^\infty \log \left\{ \frac{\gamma(y; \lambda, \beta_1)}{\gamma(y; \lambda, 1)} \right\} \gamma(y; \lambda, \beta_1) dy, \\ &= (\beta_1 - 1)\psi(\beta_1) - \log\{\Gamma(\beta_1)\}, \end{aligned} \quad (13)$$

where $\psi(\beta_1) = d \log\{\Gamma(\beta_1)\}/d\beta_1$ denotes the polygamma function of order 0, also known as the digamma function. From (13), the derivative of the Kullback–Leibler divergence is $\frac{d}{d\beta_1} \text{KLD}\{\gamma(\cdot; \lambda, \beta_1) \parallel \gamma(\cdot; \lambda, 1)\} = (\beta_1 - 1)\psi'(\beta_1)$ where $\psi'(\beta_1) = d\psi(\beta_1)/d\beta_1$ is the polygamma function of order 1. Writing $\ell(\beta_1) = \sqrt{2\text{KLD}\{\gamma(\cdot; \lambda, \beta_1) \parallel \gamma(\cdot; \lambda, 1)\}}$ we deduce that the corresponding PC prior is a mixture of two densities defined over $0 < \beta_1 < 1$ and $\beta_1 > 1$, that is,

$$\begin{aligned} \pi(\beta_1) &= \frac{\kappa_1}{2} \exp\{-\kappa_1 \ell(\beta_1)\} \left| \frac{d}{d\beta_1} \ell(\beta_1) \right| \\ &= \frac{\kappa_1}{2} \exp\left\{ -\kappa_1 \sqrt{2(\beta_1 - 1)\psi(\beta_1) - 2 \log\{\Gamma(\beta_1)\}} \right\} \left| \frac{(\beta_1 - 1)\psi'(\beta_1)}{\sqrt{2(\beta_1 - 1)\psi(\beta_1) - 2 \log\{\Gamma(\beta_1)\}}} \right|, \end{aligned} \quad (14)$$

for $\beta_1 > 0$, and where $\kappa_1 > 0$ is a predetermined penalty rate. The PC prior (14) is displayed in Figure 1 for $\kappa_1 = 1, 2, 3$. As expected, the mass is concentrated near $\beta_1 = 1$.

The prior distribution for β_2 is more conveniently constructed through the reparametrization given by the tail index $\xi = 1/\beta_2$. It makes sense to prevent very heavy tails by shrinking ξ toward zero (i.e., β_2 toward infinity), which corresponds to an exponential GP distribution in (1). Opitz et al. (2018) derived the PC-prior for ξ , which may be written as

$$\pi(\xi) = \sqrt{2\kappa_2} \exp\left\{ -\sqrt{2\kappa_2} \xi(1 - \xi)^{-1/2} \right\} (1 - \xi/2)(1 - \xi)^{-3/2}, \quad 0 < \xi < 1, \quad (15)$$

where κ_2 is the penalty rate. As (15) is compactly supported over the interval $(0, 1)$, it prevents infinite-mean models. A change of variables establishes that the PC prior for β_2 is

$$\pi(\beta_2) = \sqrt{2\kappa_2} \exp\left[-\sqrt{2\kappa_2} \{\beta_2(\beta_2 - 1)\}^{-1/2} \right] (\beta_2 - 1/2) \{\beta_2(\beta_2 - 1)\}^{-3/2}, \quad \beta_2 > 1. \quad (16)$$

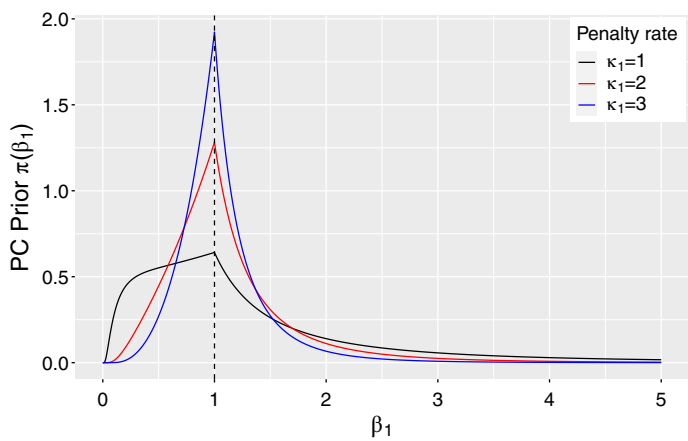


FIGURE 1 PC prior $\pi(\beta_1)$, $\beta_1 > 0$, as derived in (14), for penalty rates $\kappa_1 = 1, 2, 3$ (black, red, and blue curves, respectively)

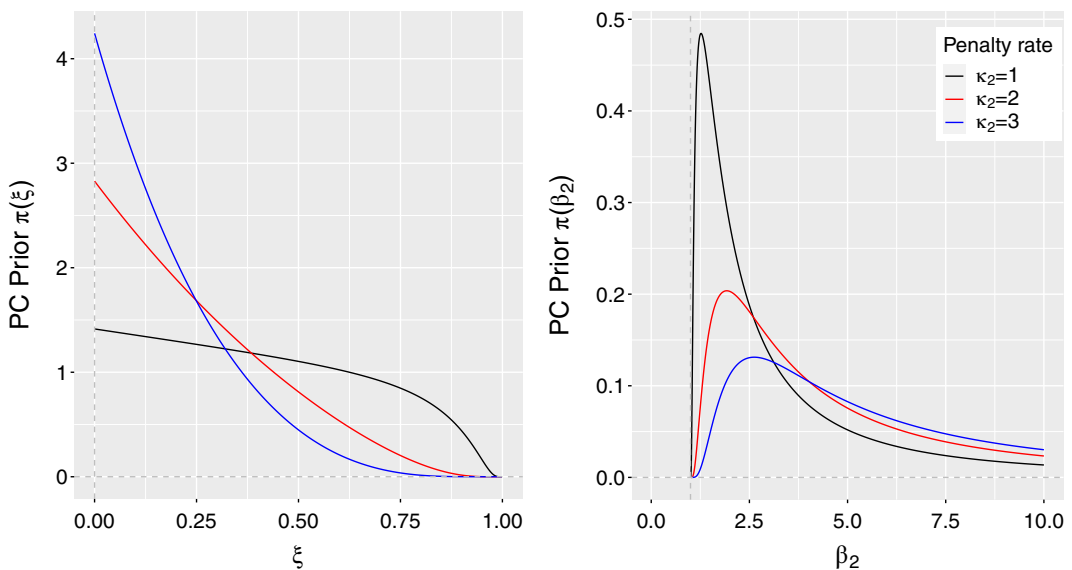


FIGURE 2 PC priors $\pi(\xi)$, $0 < \xi < 1$ (left) and $\pi(\beta_2)$, $\beta_2 > 1$ (right) as derived in (15) and (16), respectively, for penalty rates $\kappa_2 = 1, 2, 3$ (black, red, and blue curves, respectively)

Both PC priors (15) and (16) are illustrated in Figure 2 for $\kappa_2 = 1, 2, 3$. We specify vague priors for the other hyperparameters. More explicitly, we choose a gamma distribution with mean 1 and variance 100 for the correlation range ρ and a Gaussian distribution with mean 0 and variance 100 for the covariate parameters, such as $\log \alpha_0, \alpha_1, \dots, \alpha_p$ and $\log \beta_{2;0}, \beta_{2;1}, \dots, \beta_{2;q}$.

3.4 | Joint tail behavior

The upper-tail dependence in the hierarchical model with latent copula (10) is determined by the interplay between the lower joint tail of $\Lambda = (\Lambda_1, \dots, \Lambda_d)^T$ and the univariate upper tail of the distribution $F_{Y|\Lambda=1}(\cdot)$ of the independent random variables $\tilde{Y}_j, j = 1, \dots, d$, stemming from (3).

We here provide more details for the case where $1/\Lambda(s)$ has regularly varying distribution with positive tail index ξ , and \tilde{Y} is lighter-tailed such that $\mathbb{E}(\tilde{Y}^{1/\xi+\epsilon}) < \infty$ for some $\epsilon > 0$, which includes the gamma-gamma model (12). If, in addition, the multivariate distribution $F_{1/\Lambda}$ of $1/\Lambda$ is regularly varying at infinity (Resnick, 1987), we have

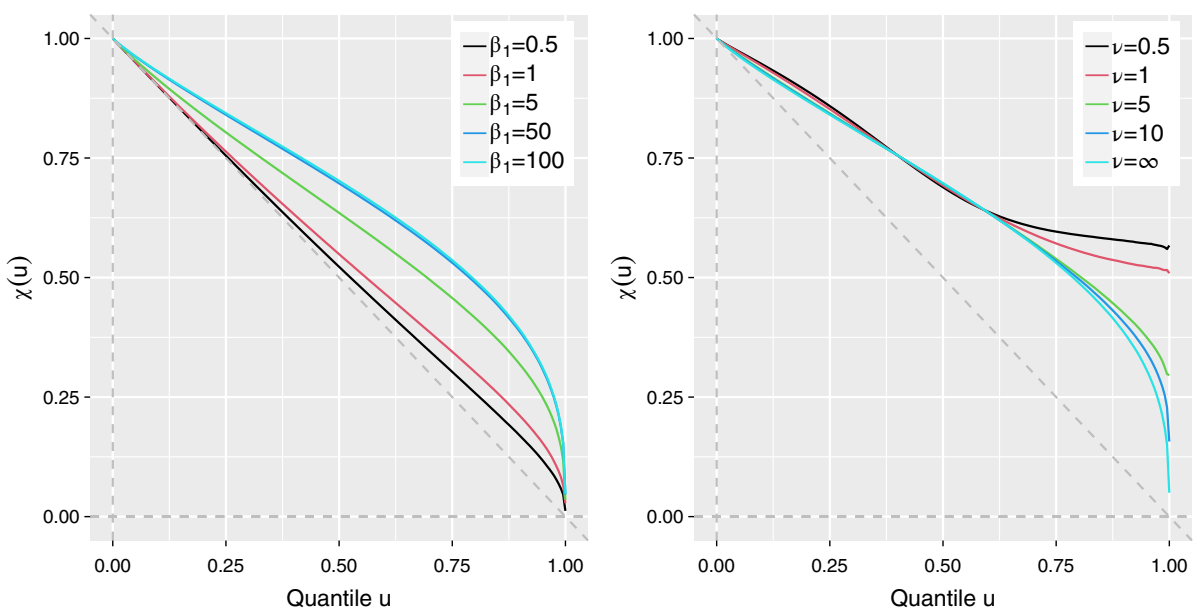


FIGURE 3 Plot of $\chi(u)$ against the quantile $u \in (0, 1)$ for the gamma–gamma model (12) at spatial distance 0.5 with latent Gaussian copula (left) and parameters $\alpha = 1, \beta_1 = 0.5, 1, 5, 50, 100, \beta_2 = 2.5$, and $\rho = 1$, and Student's t copula (right) with degrees of freedom $\nu = 0.5, 1, 5, 10, \infty$ (Gaussian) and $\alpha = 1, \beta_1 = 50, \beta_2 = 2.5$, and $\rho = 1$. The dashed diagonal gray lines correspond to exact independence

$$\frac{1 - F_{1/\Lambda}(t\mathbf{y})}{1 - F_{1/\Lambda}(t\mathbf{1})} \rightarrow V_{1/\Lambda}(\mathbf{y}), \quad \mathbf{y} > \mathbf{0}, \quad t \rightarrow \infty,$$

where $\mathbf{1} = (1, \dots, 1)^T \in \mathbb{R}^d$ and $V_{1/\Lambda}(\mathbf{y})$ is some positive limit function. Theorem 3 of Fougères and Mercadier (2012) then implies multivariate regular variation of F_Y , that is,

$$\frac{1 - F_Y(t\mathbf{y})}{1 - F_Y(t\mathbf{1})} \rightarrow V_Y(\mathbf{y}) = \int_0^\infty \dots \int_0^\infty V_{1/\Lambda}(\mathbf{y}/\mathbf{x}) \prod_{j=1}^d F_{Y|1=\mathbf{x}}(dx_j), \quad \mathbf{y} > \mathbf{0}, \quad t \rightarrow \infty. \quad (17)$$

The functions $V_{1/\Lambda}$ and V_Y are homogeneous of order $-1/\xi$, that is, $V_{1/\Lambda}(t\mathbf{y}) = t^{-1/\xi} V_{1/\Lambda}(\mathbf{y})$ and $V_Y(t\mathbf{y}) = t^{-1/\xi} V_Y(\mathbf{y})$ for positive values of t and \mathbf{y} . Equation (17) fully characterizes the extremal dependence structure of the process $Y(\mathbf{s})$ resulting from the construction (10) in the heavy-tailed case. Let $Y_1 \sim F_{Y_1}$ and $Y_2 \sim F_{Y_2}$, then a summary of the extremal dependence strength is the coefficient $\chi = \lim_{u \rightarrow 1} \chi(u)$, with $\chi(u) = \Pr\{Y_1 > F_{Y_1}^{-1}(u) | Y_2 > F_{Y_2}^{-1}(u)\}$. It can be shown that $\chi = 2 - V_Y[\{V_Y(\infty, 1)\}^\xi, \{V_Y(1, \infty)\}^\xi]$, where $\mathbf{Y} = (Y_1, Y_2)^T$. The pair of variables \mathbf{Y} is called asymptotically independent if $\chi = 0$ and asymptotically dependent if $\chi > 0$. The case of asymptotic independence corresponds to a V_Y function that is a sum of separate terms for the components, that is, $V_Y(y_1, y_2) = c(y_1^{-1/\xi} + y_2^{-1/\xi})$ with a constant $c > 0$. From (17), it follows that \mathbf{Y} is asymptotically independent if and only if $1/\Lambda = (1/\Lambda_1, 1/\Lambda_2)^T$ is asymptotically independent. Therefore the gamma–gamma model (12) with latent Gaussian copula is asymptotically independent. When the Student's t copula with $\nu > 0$ degrees of freedom is used instead, the process $Y(\mathbf{s})$ becomes asymptotically dependent (despite the conditional independence assumption at the data level).

To illustrate the dependence strength of the gamma–gamma model (12), we compute $\chi(u)$, with $u \in (0, 1)$, by simulation for different parameter values. The left panel of Figure 3 shows $\chi(u)$ obtained at spatial distance 0.5 using a latent Gaussian copula with correlation range $\rho = 1$, and the other hyperparameters set to $\alpha = 1, \beta_1 = 0.5, 1, 5, 50, 100, \beta_2 = 2.5$ (i.e., $\xi = 0.4$). The right panel of Figure 3 shows $\chi(u)$ obtained using a latent Student's t copula with range $\rho = 1$ and degrees of freedom $\nu = 0.5, 1, 5, 10, \infty$ (Gaussian), and the other hyperparameters set to $\alpha = 1, \beta_1 = 50, \beta_2 = 2.5$. These plots demonstrate that our hierarchical modeling approach can capture various joint tail decay rates and extremal dependence structures.

4 | SIMULATION-BASED BAYESIAN INFERENCE

4.1 | General strategy

We use Markov chain Monte Carlo (MCMC) sampling to generate a representative posterior sample of the hyperparameter vector Θ and the latent variables Λ involved in the hierarchical model (10), conditional on observed data. As we fit the model to threshold exceedances, we first describe the censored likelihood mechanism with latent variables in Section 4.2, focusing on the gamma–gamma model (12). Then in Section 4.3 we develop an efficient MCMC sampler by using the Metropolis-adjusted Langevin algorithm (MALA) for generating MCMC block proposals that ensure a relatively fast exploration of the high-dimensional parameter space of Λ . Also, we propose an adaptive algorithm (see Andrieu & Thoms, 2008, for an overview) to tune the calibration parameters of the MALA and random walk proposals for an appropriate convergence rate.

4.2 | Censored likelihood with latent variables

We suppose that observed data $Y_i(\mathbf{s}_j)$, $i = 1, \dots, n$, $j = 1, \dots, d$, are composed of n independent time replicates of the d components of a random vector $\mathbf{Y} = \{Y(\mathbf{s}_1), \dots, Y(\mathbf{s}_d)\}^T$ indexed by locations $\mathbf{s}_1, \dots, \mathbf{s}_d$. We discuss here inference for the spatial hierarchical gamma–gamma model with latent Gaussian copula in (12), although little would change for other hierarchical models of the form (10). We write $y_{ij} = Y_i(\mathbf{s}_j)$, $\lambda_{ij} = \Lambda_i(\mathbf{s}_j)$, $i = 1, \dots, n$, $j = 1, \dots, d$, and use the symbols ϕ and ϕ_ρ for the univariate and multivariate Gaussian densities corresponding to Φ and Φ_ρ , respectively. Given a data vector $\mathbf{y}_i = (y_{i1}, \dots, y_{id})^T$ and a fixed threshold vector $\mathbf{u}_i = (u_{i1}, \dots, u_{id})^T \in [0, \infty)^d$, we introduce the exceedance indicator vector $\mathbf{e}_i = (e_{i1}, \dots, e_{id})^T$ with $e_{ij} = 1$ if $y_{ij} \geq u_{ij}$ and $e_{ij} = 0$ otherwise. If $u_{ij} = 0$, no censoring is applied to the value y_{ij} , on the other hand, if $u_{ij} = \infty$ then the observation y_{ij} is treated as fully censored. This may be used to handle missing data and prediction at unobserved locations. We now give the augmented censored likelihood contribution of \mathbf{y}_i where we consider both Θ and $\lambda_i = (\lambda_{i1}, \dots, \lambda_{id})^T$ as parameters. The density of observations (y_{ij}, e_{ij}) conditional on λ_{ij} is $f_c(y_{ij}, e_{ij}; \lambda_{ij}, \beta_1) = \Gamma(u_{ij}; \lambda_{ij}, \beta_1)$ if $e_{ij} = 0$ and $f_c(y_{ij}, e_{ij}; \lambda_{ij}, \beta_1) = \gamma(y_{ij}; \lambda_{ij}, \beta_1)$ if $e_{ij} = 1$, where $\gamma(\cdot; \lambda_{ij}, \beta_1)$ is the gamma density with parameters λ_{ij} and β_1 . The augmented censored likelihood contribution for the data vector $(\mathbf{y}_i^T, \mathbf{e}_i^T)^T$ is thus

$$\begin{aligned} L(\Theta, \lambda_i; \mathbf{y}_i, \mathbf{e}_i) &= \prod_{j=1}^d f_c(y_{ij}, e_{ij}; \lambda_{ij}, \beta_1) \\ &\times \phi_\rho[\Phi^{-1}\{\Gamma(\lambda_{i1}; \alpha, \beta_2)\}, \dots, \Phi^{-1}\{\Gamma(\lambda_{id}; \alpha, \beta_2)\}] \times \prod_{j=1}^d \frac{\gamma(\lambda_{ij}; \alpha, \beta_2)}{\phi[\Phi^{-1}\{\Gamma(\lambda_{ij}; \alpha, \beta_2)\}]}, \end{aligned} \quad (18)$$

where the first line refers to the observation model and the second line to the latent model. The overall augmented censored likelihood is

$$L_n(\Theta, \lambda; \mathbf{y}, \mathbf{e}) = \prod_{i=1}^n L(\Theta, \lambda_i; \mathbf{y}_i, \mathbf{e}_i), \quad (19)$$

where $\lambda = (\lambda_1^T, \dots, \lambda_n^T)^T$, $\mathbf{y} = (\mathbf{y}_1^T, \dots, \mathbf{y}_n^T)^T$, and $\mathbf{e} = (\mathbf{e}_1^T, \dots, \mathbf{e}_n^T)^T$. Notice that thanks to data augmentation and to the conditional independence assumption, only univariate censoring is required, hence facilitating computations.

4.3 | Metropolis–Hastings MCMC algorithm with adaptive MALA and random walk proposals

We implement a Metropolis–Hastings MCMC algorithm to sample from the posterior distribution of hyperparameters Θ and latent variables $\lambda = (\lambda_1^T, \dots, \lambda_n^T)^T$. More precisely, we update the parameters Θ and λ in two separate blocks for a predetermined number of iterations, in order to construct a Markov chain whose stationary distribution is the posterior distribution of interest. To avoid invalid proposals or strong dependence between posterior samples of latent parameters or

hyperparameters, we first apply the following reparametrization of the model: the latent parameters are log-transformed, that is, $\tilde{\lambda} = \log(\lambda)$, while the hyperparameters of the gamma–gamma model (12) are reparametrized (internally) as

$$\tilde{\alpha} = \log(\alpha\beta_1/\beta_2), \quad \tilde{\beta}_1 = \log(\alpha\beta_1^2/\beta_2), \quad \tilde{\beta}_2 = \log(1/\beta_2), \quad \tilde{\rho} = \log(\rho). \quad (20)$$

The reverse transformation is $\alpha = \exp(2\tilde{\alpha})\exp(-\tilde{\beta}_1)\exp(-\tilde{\beta}_2)$, $\beta_1 = \exp(-\tilde{\alpha})\exp(\tilde{\beta}_1)$, $\beta_2 = \exp(-\tilde{\beta}_2)$, $\rho = \exp(\tilde{\rho})$. To use this modified internal reparametrization, we correct the target posterior density $\pi_{\text{post}}(\Theta, \lambda | \mathbf{y}, \mathbf{e}) \propto L_n(\Theta, \lambda; \mathbf{y}, \mathbf{e})\pi(\Theta)$ through the determinant of the Jacobian matrix of the transformation; its value is $\exp(\tilde{\rho} + \tilde{\alpha} - 2\tilde{\beta}_2)$ for the hyperparameter transformation in (20).

Our proposed MCMC algorithm consists of the following steps: we iteratively propose candidate values for the transformed hyperparameters $\tilde{\Theta}$ and latent parameters $\tilde{\lambda}$ from some proposal densities $q_1(\tilde{\Theta}' | \tilde{\Theta})$ and $q_2(\tilde{\lambda}' | \tilde{\lambda})$, respectively, and we accept these candidates with probability

$$\min \left(1, \frac{L_n(\tilde{\Theta}', \tilde{\lambda}; \mathbf{y}, \mathbf{e}) \pi(\tilde{\Theta}') q_1(\tilde{\Theta} | \tilde{\Theta}')}{L_n(\tilde{\Theta}, \tilde{\lambda}; \mathbf{y}, \mathbf{e}) \pi(\tilde{\Theta}) q_1(\tilde{\Theta}' | \tilde{\Theta})} \right), \quad \min \left(1, \frac{L_n(\tilde{\Theta}, \tilde{\lambda}'; \mathbf{y}, \mathbf{e}) q_2(\tilde{\lambda}' | \tilde{\lambda}')}{L_n(\tilde{\Theta}, \tilde{\lambda}; \mathbf{y}, \mathbf{e}) q_2(\tilde{\lambda}' | \tilde{\lambda})} \right),$$

for hyperparameters and latent parameters, respectively. The number of parameters (latent variables and hyperparameters) to be explored by the Markov chain is equal to $N = nd + l$, with $l = |\tilde{\Theta}|$. In particular, it grows linearly with the sample size n and dimension d . To handle the high dimensionality of the vector of latent variables, we propose using the Metropolis-adjusted Langevin algorithm (MALA), which exploits the gradient of the log-posterior density evaluated at the current parameter configuration to design an efficient multivariate Gaussian proposal density $q_2(\tilde{\lambda}' | \tilde{\lambda})$. Because the number of hyperparameters is moderate, we specify simple random walk proposals for $q_1(\tilde{\Theta}' | \tilde{\Theta})$. Specifically, we propose candidate values $\tilde{\Theta}'$ and $\tilde{\lambda}'$ consecutively as follows:

$$\begin{aligned} \tilde{\Theta}' | \tilde{\Theta} &\sim \mathcal{N}(\tilde{\Theta}, \tau_\Theta I_l), \\ \tilde{\lambda}' | \tilde{\Theta}, \tilde{\lambda} &\sim \mathcal{N}(\tilde{\lambda} + \tau_\lambda \nabla_{\tilde{\lambda}} \log \pi_{\text{post}}(\tilde{\Theta}, \tilde{\lambda} | \mathbf{y}, \mathbf{e}), 2\tau_\lambda I_{nd}), \end{aligned}$$

where I_l and I_{nd} are the identity matrices of dimensions $l \times l$ and $nd \times nd$, respectively, and $\tau_\Theta > 0$ and $\tau_\lambda > 0$ are step sizes controlling the variance of q_1 and q_2 , respectively. In our proposed model, the gradient of the log-posterior density can be obtained in closed form, facilitating inference; see the details in the Supplementary Material.

We use two burn-in phases in our MCMC algorithm. During the initial burn-in phase, we adapt the tuning parameters τ_Θ and τ_λ as follows. Let τ_{cur} denote the current value of either τ_Θ or τ_λ , P_{acc} be the current acceptance probability calculated from the last 500 iterations, and P_{tar} be a target acceptance probability. Every 500 iterations, we update τ_{cur} as $\tau_{\text{cur}} \mapsto \tau_{\text{new}} := \exp\{(P_{\text{acc}} - P_{\text{tar}})/\omega\}\tau_{\text{cur}}$, where ω controls the rate of change. Here, we set $P_{\text{tar}} = 0.57$ for τ_λ , which was found to be optimal for the MALA algorithm under independence assumptions (Roberts & Rosenthal, 1998), and $P_{\text{tar}} = 0.23$ for τ_Θ , which usually works well for random walks. Moreover, we here fix ω to 0.4. In the second burn-in phase, we use the same adaptive scheme only if the acceptance probability drops out of the intervals $[0.50, 0.65]$ and $[0.15, 0.30]$ for MALA and random walk proposals, respectively, that is, if it has not stabilized yet during the initial burn-in phase. In all simulation experiments, we use a total of 1,500,000 iterations, with 250,000 iterations for the initial burn-in phase, and 500,000 iterations for the second burn-in phase, whereas for the data application we doubled the length of all phases.

5 | SIMULATION STUDY

5.1 | Simulation scenarios

In this section, we study the performance of our MCMC sampler under diverse simulation scenarios. Data are simulated from the gamma–gamma model (12) with latent copula model for $d \in \{50, 100, 200, 400\}$ spatial locations sampled at random (i.e., uniformly) in the unit square $[0, 1]^2$, with $n \in \{50, 100, 200, 250\}$ temporal replicates, depending on the scenario. The latent process $\Lambda(\mathbf{s})$ has a Gaussian or Student's t copula with isotropic exponential correlation function $\sigma(\mathbf{s}_i, \mathbf{s}_j) = \exp\{-(\|\mathbf{s}_i - \mathbf{s}_j\|/\rho)\}$, $\rho > 0$. In some cases, we apply the censoring scheme presented in Section 4.2, using

site-specific thresholds chosen as the empirical 75%-quantile. When performing spatial prediction, we set the censoring threshold to $+\infty$.

To be concise, we here only discuss the results for one scenario, and we report the results for all scenarios in the Supplementary Material. Specifically, we here consider $d = 100$ spatial locations (80 used for fitting, and 20 kept for spatial prediction), $n = 100$ temporal replicates, and we use a latent Gaussian copula with range $\rho = 1$. We assume that the marginal scale parameter depends on spatially varying covariates in log-linear specification, such that $\alpha(\mathbf{s}) = \alpha_0 \exp\left\{\sum_{k=1}^3 \alpha_k z_k(\mathbf{s})\right\}$, with covariates $z_1(\mathbf{s})$ and $z_2(\mathbf{s})$ corresponding to the x and y coordinates of the location \mathbf{s} , respectively, and $z_3(\mathbf{s})$ being generated as a Gaussian random field model with mean 0, variance 1, and correlation $\sigma_{ij} = \exp(-\|\mathbf{s}_i - \mathbf{s}_j\|/2)$. This setting is similar to the setting considered in the application in Section 6. The regression coefficients are set to $\alpha_0 = \alpha_1 = \alpha_2 = \alpha_3 = 1$ and the other hyperparameters are fixed to $\beta_1 = 5$ and $\beta_2 = 5$ (i.e., with tail index $\xi = 0.2$).

We use the adaptive MCMC algorithm developed in Section 4.3. We run two MCMC chains with different initial values in parallel to check the dependence on initial conditions, and we then calculate MCMC outputs by combining these two chains.

5.2 | Results

Figure 4 displays the trace plots for all the hyperparameters and one selected latent variable, for two MCMC chains with different initial values. The results show that there is good mixing and that convergence occurs very quickly for the regression parameters α_0 , α_1 , α_2 , and α_3 , and relatively quickly for the other hyperparameters or latent variables, despite the large number of latent variables. Essentially in this scenario, all Markov chains seem to have converged after about 350,000 to 500,000 iterations. For all parameters, the true value lies well within the corresponding posterior distribution, confirming the good performance of our algorithm. The effective sample size per minute is roughly between 10 and 60, see Table 1 in the Supplementary Material. The proposal variances, automatically tuned in our algorithm, converged to the values $\tau_\Theta = 1.2 \times 10^{-4}$ for the hyperparameters (based on random walk proposals) and $\tau_\lambda = 5.4 \times 10^{-4}$ for the latent variables (based on MALA proposals). The total run time for each Markov chain is almost 1.5 days to achieve 1.5 million iterations.

We then study the ability of our model to predict values at unobserved locations. To this end, we treat the data at 20 randomly selected sites as missing, and we compute the posterior predictive distributions at these sites. Figure 5 compares boxplots of the true simulated values at the 20 prediction sites to posterior predictive samples obtained from fitting our model. Clearly, the posterior predictive distributions at all prediction sites appropriately capture the natural variability in the true data. This suggests that our algorithm succeeds in performing spatial prediction. The great benefit of our Bayesian approach is that estimation based on censored data and spatiotemporal prediction are performed simultaneously.

6 | APPLICATION TO PRECIPITATION EXTREMES FROM GERMANY

6.1 | Data description

We now study precipitation intensities observed in Germany, publicly available from the European Climate Assessment & Dataset project. The dataset reports daily precipitation amounts observed at more than 5000 spatial locations during the period 1941 to 2018. We apply our hierarchical models to a subset of $d = 150$ locations with some missing data for the study period from 2009 to 2018. To avoid modeling complex seasonal nonstationarities, we consider the observations for the (full) months of September to December (i.e., for the extended autumn season), resulting in $n = 1220$ temporal replicates. This time period was merely selected based on temporal stationarity diagnostics, although from a practical perspective it would also be interesting in future research to extend our stationary models in order to study seasonal patterns in precipitation intensities during other months, as well as to assess the flood risk all year round. The site-specific mean precipitation intensities reported in Figure 6 show a tendency toward higher values in regions with higher altitudes; see Murawski et al. (2016) for more details about spatial and temporal trends in precipitation over Germany. In a preliminary analysis of the tail behavior of precipitation intensities, we fit the GP distribution to exceedances at each site

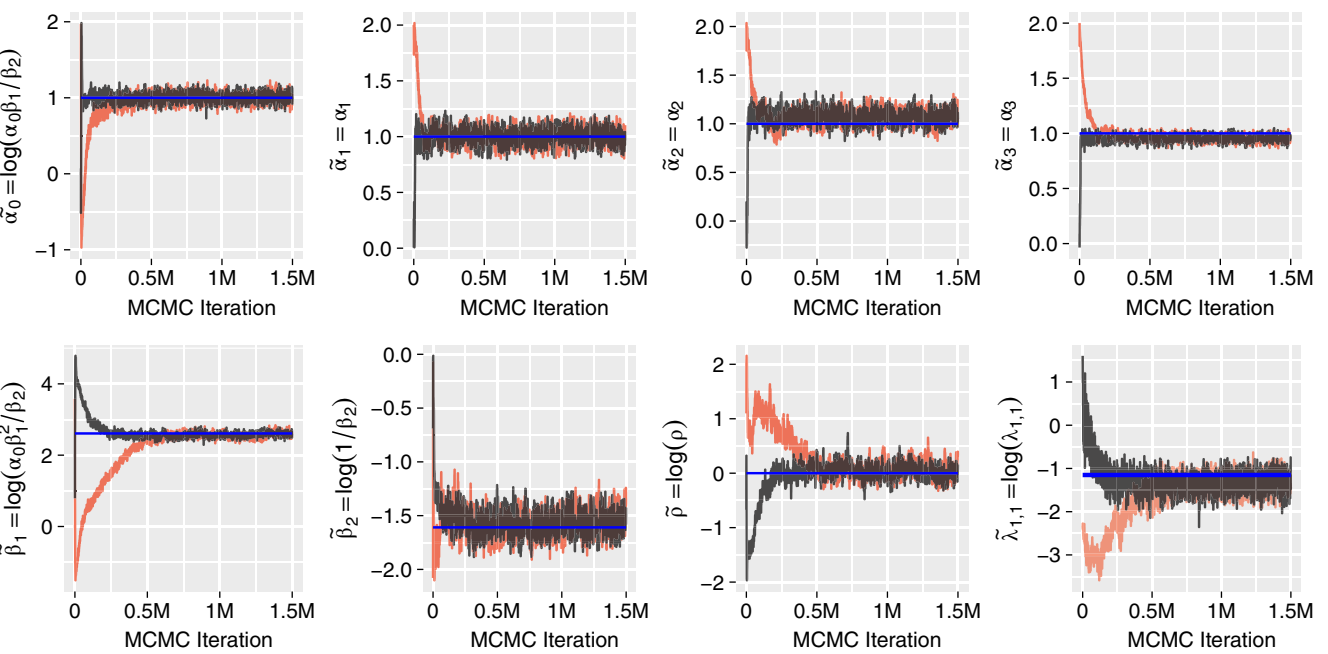


FIGURE 4 Trace plots for the simulation scenario detailed in Section 5.1, where the hyperparameters are set to $\alpha_0 = \alpha_1 = \alpha_2 = \alpha_3 = 1$, $\beta_1 = 5$, $\beta_2 = 5$ (i.e., $\xi = 0.2$), and $\rho = 1$. The rightmost plot in the second row corresponds to one chosen latent parameter, and the remaining seven plots are for all the hyperparameters. The red and black chains are two MCMC samples with different initial values, and the horizontal blue line represents the true values of the parameters. The total number of MCMC samples is 1,500,000

separately with site-specific thresholds fixed at the 85% empirical quantile of positive precipitation intensities. The maximum likelihood estimator, and the moment-based estimator of Dekkers et al. (1989) of the tail index, both provide systematically positive tail index estimates. This finding suggests that precipitation intensities are heavy-tailed as expected, and we proceed by fitting the spatial gamma-gamma model (12) to selected extreme precipitation events (see Section 6.3). The selection of extreme events and the modeling of their occurrences are described in Section 6.2.

6.2 | Identifying and modeling extreme precipitation occurrences

The precipitation intensities are zero or very small for most of the days in the observation period, and we first extract extreme events (i.e., specific days) used to fit our spatial hierarchical model. Let $Y_t(\mathbf{s}_j)$ denote the precipitation intensities at time t and site \mathbf{s}_j , $j = 1, \dots, d$. To select extreme events, we consider the spatial average precipitation $S_t = d^{-1} \sum_{j=1}^d Y_t(\mathbf{s}_j)$, indexed by time t . We then define extreme events as days t such that $S_t > \hat{G}^{-1}(0.85)$, where \hat{G} is the empirical cumulative distribution function of the sample of S_t values. This scheme extracts 181 extreme events in total.

Let $E_{a,t}$ denote the binary sequence of 0 and 1 values representing the occurrence indicators of extreme events for the a -th year, with $a \in \{1, \dots, 10\}$. That is, $E_{a,t} = 1$ if the t -th day of the year, with $t \in \{244, \dots, 365\}$, was extreme in year a , and $E_{a,t} = 0$ otherwise. To capture temporal dependence, we model this time series through a logistic regression with a random effect defined as a first-order autoregressive Gaussian process, that is,

$$\begin{aligned} \log \left\{ \frac{\Pr(E_{a,t} = 1)}{1 - \Pr(E_{a,t} = 1)} \right\} &= \beta_{E,0} + W_{a,t}, \\ W_{a,1} &\stackrel{\text{iid}}{\sim} \mathcal{N}(0, \sigma_E^2 / (1 - \rho_E^2)), \quad a = 1, \dots, 10, \\ W_{a,t} | W_{a,t-1} &= \rho_E W_{a,t-1} + \varepsilon_{a,t}, \quad t = 244, \dots, 365, \\ \varepsilon_{a,t} &\stackrel{\text{iid}}{\sim} \mathcal{N}(0, \sigma_\varepsilon^2), \end{aligned} \tag{21}$$

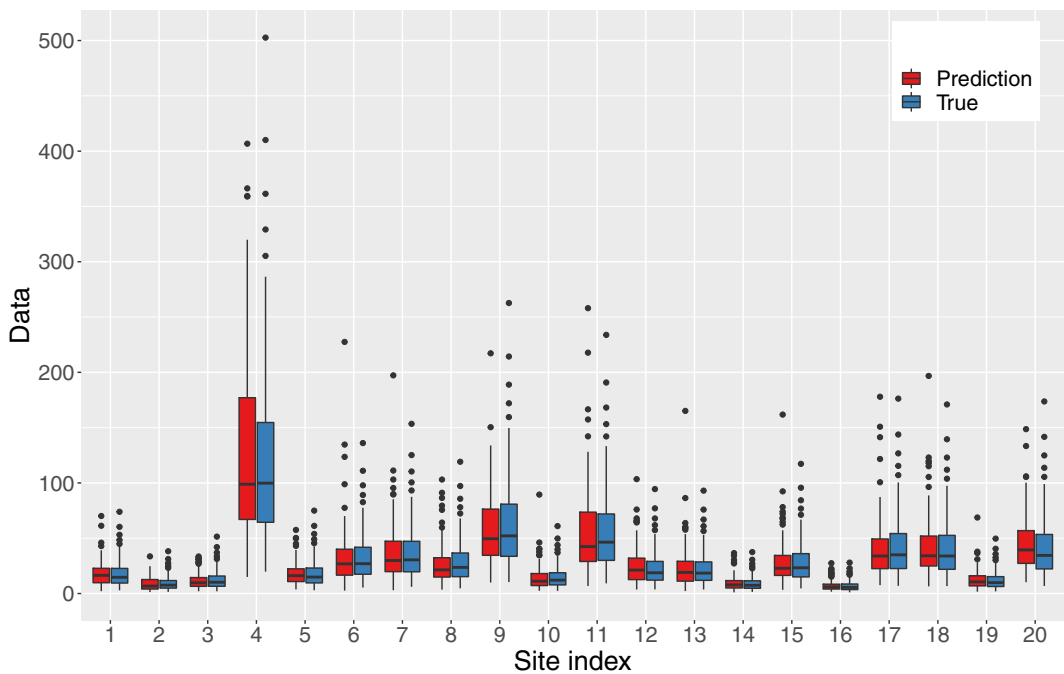


FIGURE 5 Boxplots of the posterior predictive samples (red) and true observations (blue) at all the prediction sites, for the simulation scenario described in Section 5.1. The total number of MCMC samples is 1,500,000, and the posterior samples are derived from the last 750,000 MCMC samples, obtained after removing the initial 750,000 burn-in samples

with global intercept $\beta_{E,0}$, autoregression coefficient $\rho_E \in (-1, 1)$, and marginal variance of $W_{a,t}$, $\sigma_E^2 = \sigma_e^2/(1 - \rho_E^2) > 0$. We have explored a number of alternative models including an additional seasonal trend component in the regression equation (21), but we could not detect any significant improvement with respect to model (21).

We now present the estimation results for model (21). While there would be no notable obstacles for MCMC-based estimation of this model, we here propose using the integrated nested Laplace approximation (INLA, Rue et al., 2017) implemented in the INLA package of the statistical software R. It provides fast and “off-the-shelf” Bayesian inference for logistic regression models such as (21). We obtain the following parameter estimates, with 95% credible intervals in parentheses:

$$\hat{\beta}_{E,0} = -2.4 (-2.8, -2.0), \quad \hat{\rho}_E = 0.76 (0.63, 0.85), \quad \hat{\sigma}_E^2 = 2.1 (1.1, 3.5).$$

The estimated negative value of $\beta_{E,0}$ indicates that there is a higher probability for nonextreme events, as expected, while the estimated value of ρ_E suggests that there is some nonnegligible temporal persistence of zeros and ones. Figure 7 shows the fitted probability values for a selection of 4 years (1, 2, 9, 10). The fitted models suggest relatively strong temporal autocorrelation: an extreme event at time t entails an extreme event at time $t + 1$ with probability substantially above average.

6.3 | Modeling extreme precipitation intensities

We now return to the modeling of (nonzero) precipitation intensities, and we fit the gamma–gamma model (12) with latent Gaussian copula to the time series of selected extreme events. The model structure and data dimension are similar to those considered in the simulation study in Section 5. We use standardized latitude, longitude, and altitude as covariates in the model. The dataset of extreme events is composed of $d = 150$ sites and $n = 181$ days, leading to $nd = 27,150$ (spatially correlated) latent variables in the model. The minimum and maximum distances between the selected sites are 6 and 819 km, respectively. We use 20 sites for prediction and model validation (where the data are treated as completely missing). The remaining 130 sites are used for model fitting. The proportion of missing observations at each of

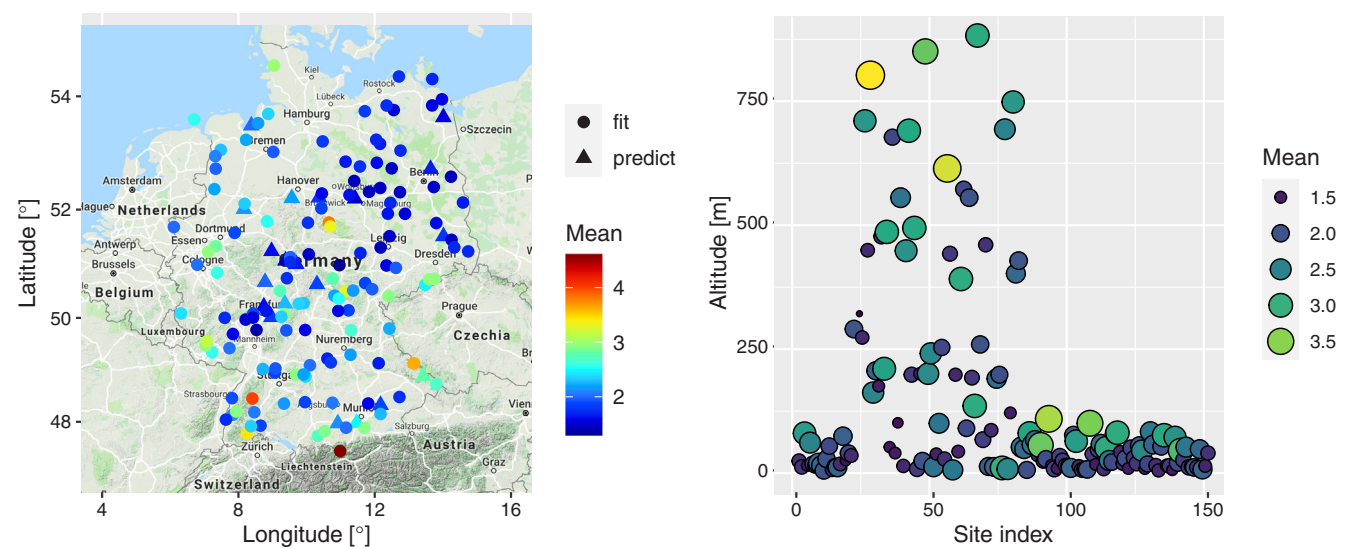


FIGURE 6 Left: Mean precipitation (mm) at the study sites calculated over the days corresponding to the selected extreme events; see Section 6.2. Right: Mean precipitation (mm) plotted with respect to the station's altitude (m). For visibility purposes, we do not show the station at the highest altitude (≈ 3000 m) on the right panel

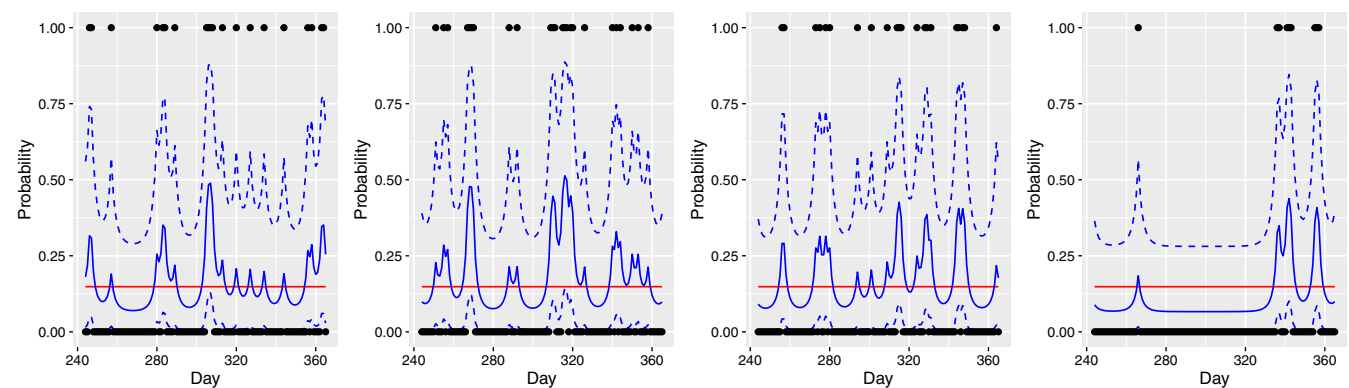


FIGURE 7 Posterior estimates (fitted probability values) of observing an extreme event at a given day according to model (21) for the years 1, 2, 9, 10 (from left to right). Black \bullet symbols indicate the observations $E_{a,t}$. Posterior means and 95% credible intervals of $\Pr(E_{a,t} = 1)$ are reported by continuous and dashed blue curves, respectively. The red line indicates the global empirical exceedance probability equal to 0.15

the 130 training sites varies from 1% to 10%, for an average of 3%. Our goal is also to compare how our model performs at different marginal thresholds, in order to assess the flexibility of our “subasymptotic” modeling approach, and we consider empirical quantiles at three moderately large probability levels, namely 85%, 90%, and 95%. Notice that while zero precipitation values may still occur at some spatial sites during extreme events, which creates a point mass at the lower endpoint of the precipitation distribution, we here avoid the tricky explicit treatment of zeros by censoring low precipitation intensities. We fit four different spatial models to the precipitation events obtained in Section 6.2, namely:

- D1 Gamma–gamma model (12) with standardized spatial covariates given by latitude, longitude, and altitude included in the scale parameter α .
- D2 Gamma–gamma model (12) with standardized spatial covariates given by latitude, longitude, and altitude included in both the scale α and shape β_2 parameters.
- D3 Exponential–gamma (i.e., GP unconditionally) model, akin to Bopp and Shaby (2017), with standardized spatial covariates given by latitude, longitude, and altitude included in the scale parameter α . This model may be obtained from Model D1 by fixing $\beta_1 = 1$.

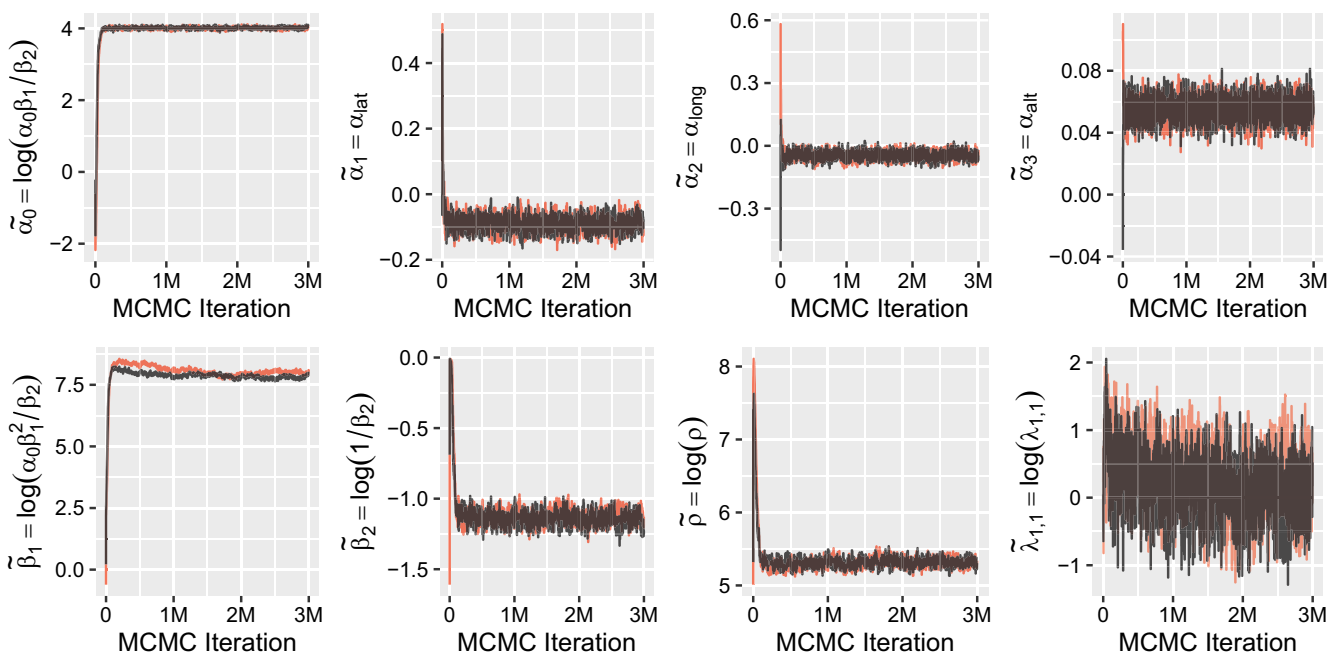


FIGURE 8 Trace plots of the seven hyperparameters, and of a selected latent variable (lower right plot) for model D1. The marginal censoring threshold is here set to 90%. The red and black curves show two MCMC samples with different initial values. The total number of MCMC samples is 3,000,000

D4 Exponential-gamma (i.e., GP unconditionally) model, akin to Bopp and Shaby (2017), with standardized spatial covariates given by latitude, longitude, and altitude included in both the scale α and shape β_2 parameters. This model may be obtained from Model D2 by fixing $\beta_1 = 1$.

We fit all four models using the MCMC algorithm detailed in Section 4. We chose random initial values for all the hyperparameters, while we used the copula structure of latent variables defined in (12) to generate initial values for the latent parameters. The trace plots displayed in Figure 8 show two MCMC chains with different initial values for all the hyperparameters and the latent parameter $\tilde{\lambda}_{1,1} = \log(\lambda_{1,1})$ (site 1, day 1) for model D1 with censoring threshold 90%. The behavior of the chains for the other latent variables is similar to $\tilde{\lambda}_{1,1}$. The Markov chains for the other models (D2, D3, D4) and for different censoring thresholds (85%, 90%, 95%) are similar to those displayed in Figure 8; see Figures 9, 10, 13, 15, and 17 in the Supplementary Material. The chains mix satisfactorily and converge to their stationary distribution after about 150,000–500,000 iterations for most parameters. Figure 7 in the Supplementary Material shows trace plots of the tuning parameters τ_λ and τ_Θ for the MALA and random walk proposals, respectively. The tuning parameters stabilize well before the end of the first burn-in phase of 750,000 iterations, which illustrates the good performance of our adaptive MCMC algorithm.

In Table 1, we compare models based on the continuous ranked probability score (CRPS) (Gneiting & Raftery, 2007) and the tail weighted continuous ranked probability score (twCRPS) (Lerch et al., 2017) for all the models (D1, D2, D3, and D4) and for different censoring thresholds (85%, 90%, and 95%). While the CRPS is a proper scoring rule widely used to assess calibration and sharpness of probabilistic forecasts, the twCRPS is similar but focuses on the largest fraction of the data only (i.e., the upper tail). Based on the CRPS, model D1 appears to be the best among the four models considered, with much better scores than the exponential-gamma models (D3 and D4) and slightly better scores than the gamma-gamma model with covariates included both in the scale α and the shape β_2 . However, based on the twCRPS, model D2 appears to be comparable to, yet still slightly better than model D1. Since model D1 is more parsimonious and easier to fit, has only a slight difference in twCRPS compared to model D2, and avoids issues of poor tail index predictions at unobserved sites (e.g., for unusual covariate values), we consider model D1 as our “best” model overall for our modeling extreme precipitation data over Germany. For brevity, we here only present the results for model D1; see the Supplementary Material for more details on the other models. Table 2 reports posterior mean estimates and two-sided 95% credible intervals for all hyperparameters and some latent parameters for model D1. Interestingly, the results are

TABLE 1 CRPS and twCRPS values for all the candidate models, where the weight function in twCRPS is the Gaussian distribution function with variance 25 and mean as the corresponding marginal threshold values

Model\Threshold	CRPS			twCRPS		
	85%	90%	95%	85%	90%	95%
D1	35.32	35.46	35.56	9.17	6.77	3.95
D2	35.39	35.60	35.71	9.05	6.72	3.90
D3	39.55	40.21	42.07	9.23	6.79	3.95
D4	39.65	40.31	42.25	9.23	6.80	3.95

Note: Lower values of CRPS and twCRPS are better. For each threshold and each diagnostic (CRPS/twCRPS), the best performance is highlighted in bold.

TABLE 2 Posterior mean (post. mean) and 95% credible interval (CI) of hyperparameters and of several latent parameters, reported for the censoring thresholds 85%, 90%, and 95%

Threshold	85%		90%		95%	
	Parameter	Post. mean	95% CI	Post. mean	95% CI	Post. mean
α_0	1.16	(1.04, 1.30)	1.27	(1.16, 1.38)	1.39	(1.23, 1.51)
α_{lat}	-0.09	(-0.12, -0.06)	-0.09	(-0.12, -0.06)	-0.09	(-0.13, -0.06)
α_{long}	-0.05	(-0.07, -0.03)	-0.05	(-0.07, -0.02)	-0.05	(-0.08, -0.02)
α_{alt}	0.06	(0.05, 0.06)	0.05	(0.05, 0.06)	0.05	(0.04, 0.06)
β_1	48.53	(42.33, 53.00)	48.55	(44.43, 51.55)	45.94	(42.36, 50.43)
ξ	0.34	(0.32, 0.37)	0.32	(0.30, 0.34)	0.30	(0.28, 0.33)
ρ	203.02	(187.47, 220.14)	205.15	(189.33, 223.24)	212.87	(189.82, 234.22)
$\lambda_{1,1}$	0.85	(0.51, 1.31)	1.26	(0.67, 2.08)	1.02	(0.54, 1.72)
$\lambda_{6,95}$	0.39	(0.26, 0.54)	0.37	(0.25, 0.52)	0.32	(0.21, 0.46)
$\lambda_{56,95}$	0.71	(0.45, 1.06)	0.62	(0.41, 0.92)	0.80	(0.43, 1.36)

Note: The tail index parameter ξ is equal to $1/\beta_2$. The total number of MCMC iterations is 3,000,000. Estimations are based on the last 1,500,000 MCMC samples, obtained after removing the first 1,500,000 burn-in samples.

fairly consistent across marginal censoring thresholds, indicating that our subasymptotic model can flexibly accommodate departure from the asymptotic GP distribution at finite levels; see also Figure 9, which compares boxplots of posterior predictive samples at all prediction sites for the three different censoring thresholds, 85%, 90%, and 95%. As the conclusions are quite robust to the choice of the threshold, we now discuss the results for the 90% threshold. The effect of the three covariates (latitude, longitude, altitude) is always significant as the 95% credible intervals do not include 0. This result demonstrates the importance of including suitable geographical information in the scale parameter α of the distribution. The estimates for latitude ($\hat{\alpha}_{\text{lat}} = -0.09$) and longitude ($\hat{\alpha}_{\text{long}} = -0.05$) indicate that the south-western part of Germany receives higher precipitation amounts than the north-eastern part—a pattern that is clearly perceptible in the mean precipitation plot in left panel of Figure 6. Moreover, a clear positive effect of higher altitude on precipitation amounts arises with an estimate of ($\hat{\alpha}_{\text{alt}} = 0.05$), which is also clear from the right panel of Figure 6. The estimate of the shape parameter β_1 is around 49 and shows a huge difference with respect to the generalized Pareto model with $\beta_1 = 1$. This finding substantiates our claim that extensions to the generalized Pareto distribution are useful for capturing complex data behavior at subasymptotic levels, and it confirms the comparison of models in Table 1. The estimated tail index $\hat{\xi}$ at the 90% censoring threshold is about 0.32, which corresponds to quite heavy tails. The estimated range parameter $\hat{\rho}$ of the exponential correlation function is around 205 km, implying a correlation of approximately 0.95 at the latent level between two sites separated by 10 km. This correlation decreases to approximately 0 between the two furthest sites.

We now illustrate the spatial predictive performance of model D1 by QQ-plots and boxplots; see the Supplementary Material for diagnostics on the performance of the other models. To be concise, we here only discuss the results for the marginal censoring threshold 90%; see Figure 10. The results for the other marginal thresholds are similar and reported

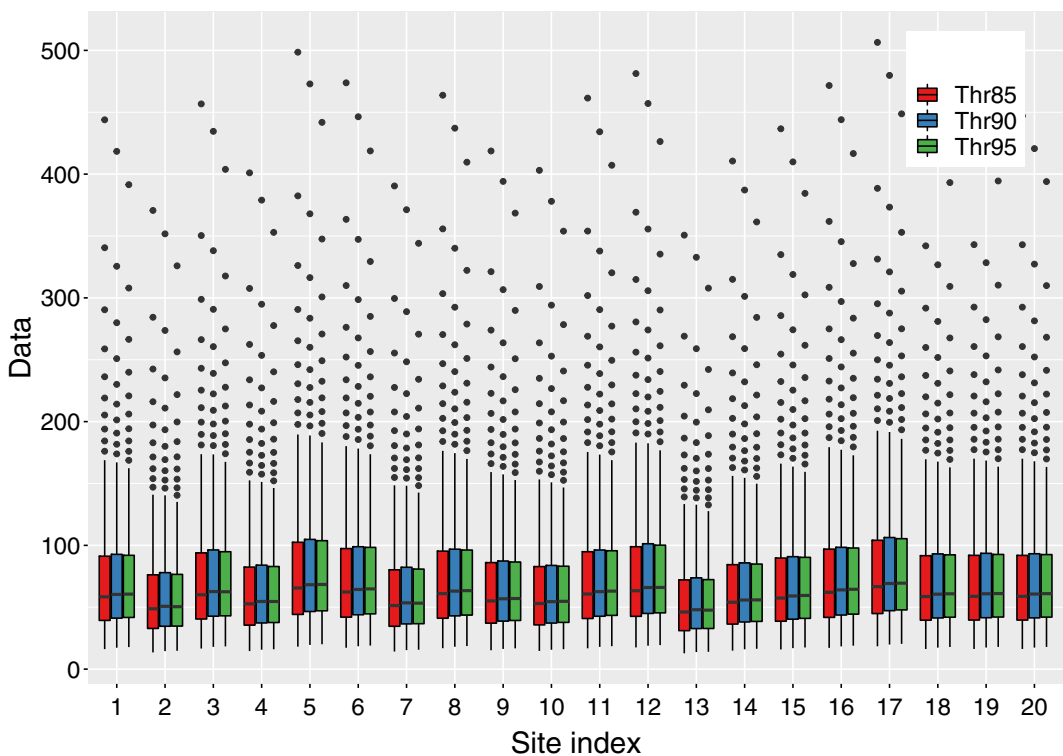


FIGURE 9 Boxplots of posterior predictive samples at all prediction sites from model D1 fitted to exceedances of the three different censoring thresholds (Thr) 85%, 90%, and 95%. The total number of MCMC samples is 3,000,000, and the boxplots are based on the last 1,500,000 MCMC samples, obtained after removing the first 1,500,000 burn-in samples

in the Supplementary Material. The first four rows in Figure 10 correspond to the 20 prediction sites, which are treated as fully missing, and the last row displays QQ-plots for five randomly chosen sites used for fitting the model. We use the prediction sites to assess whether our fitted model appropriately predicts marginal distributions at unobserved sites. The model quantiles displayed in these QQ-plots are based on the unconditional $(\hat{\alpha}\hat{\beta}_1/\hat{\beta}_2)F_{2\hat{\beta}_1,2\hat{\beta}_2}$ distribution, where $\hat{\alpha}$, $\hat{\beta}_1$, and $\hat{\beta}_2$ are posterior mean estimates of α , β_1 , and β_2 for each site, respectively. We obtain 95% uncertainty bands in the QQ-plots using a parametric bootstrap procedure accounting for missing values. Overall, the spatial predictive performance of model D1 is quite good, except perhaps at the prediction site 3, where our model tends to underestimate the empirical quantiles. Similar results were obtained for model D2 and other censoring levels with a generally satisfactory performance from low to high quantiles, but results are much worse for the exponential-gamma models D3 and D4; see the Supplementary Material for details. Boxplots of posterior predictive distributions based on model D1 for all prediction sites (see Figure 8 of the Supplementary Material), roughly correspond to the empirical distribution of the data available at these sites, though with a slightly larger variability as expected. This suggests that our model is able to adequately capture the natural variability of precipitation intensities at unobserved locations. Based on our graphical diagnostics, model D1 seems to be the best overall to predict the precipitation distribution at unobserved locations. Furthermore, our results illustrate how the spatial dependence structure assumed at the latent level in our model can help predict precipitation over space.

In summary, we conclude that our model appropriately captures spatial trends and dependence patterns of precipitation intensities during the extended autumn season in Germany. Specifically, it provides useful probabilistic predictions at unobserved locations during extreme events.

7 | CONCLUSION

We have proposed several univariate models extending the generalized Pareto limit model for threshold exceedances, and studied their tail properties. The high flexibility of these models suggests that they are good candidates for threshold-based

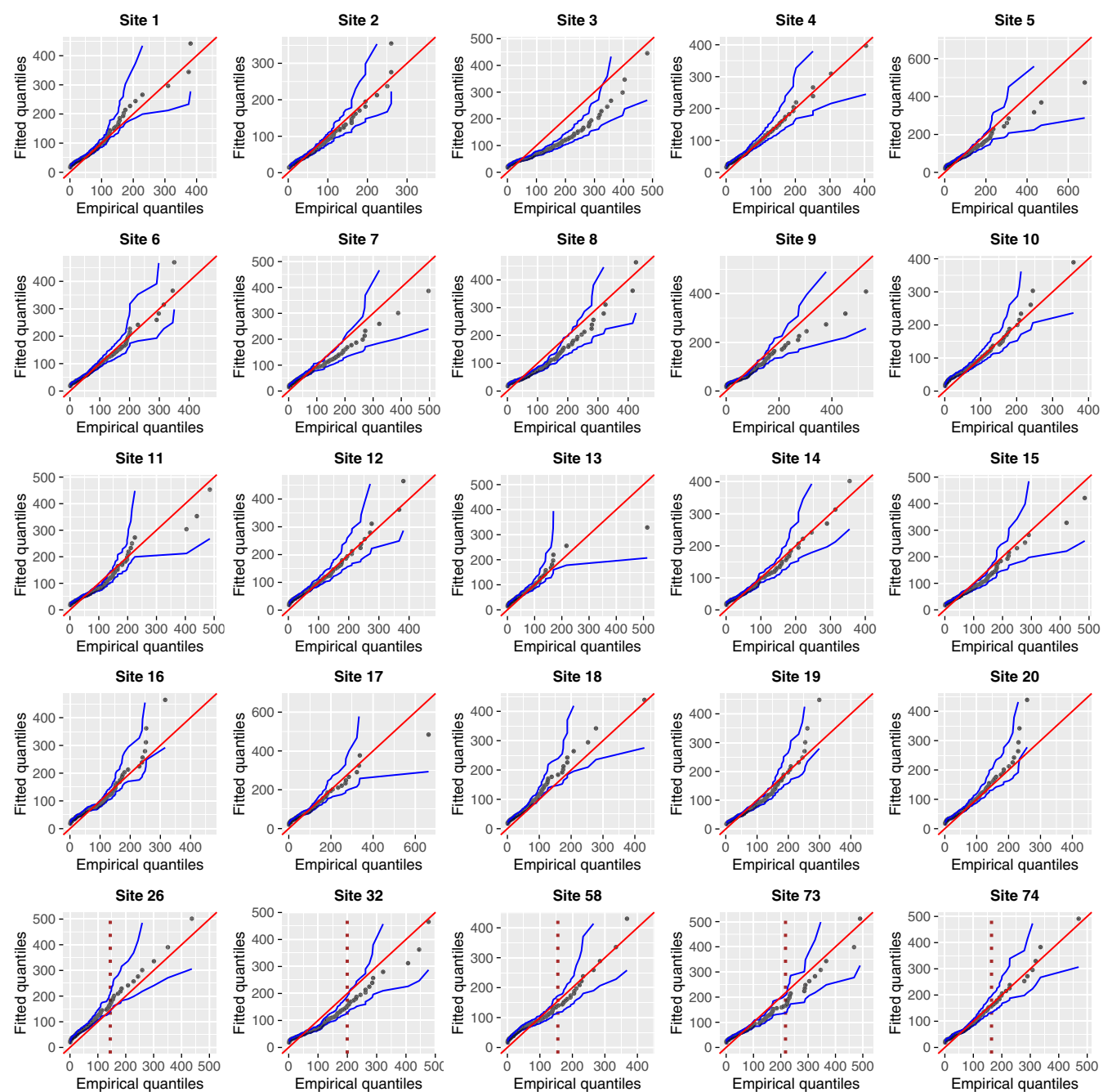


FIGURE 10 QQ-plots for all prediction sites for which the censoring threshold is set to $+\infty$ (top four rows), and some randomly chosen sites used for fitting the model (last row), based on model D1. Here, the marginal censoring thresholds are set to 90%. The vertical dotted brown lines in the last row indicate the threshold values. The QQ-plots are obtained by comparing the empirical data quantiles to the fitted quantiles calculated by plugging the posterior mean estimates into the unconditional F -distribution

modeling of moderate to large values. Our models are based on hierarchical constructions using latent processes for spatial dependence. In this way, they avoid the artificial and overly strong separation of marginal and dependence modeling often encountered in spatial extreme-value analysis.

Our Bayesian estimation approach bears witness of the power of the MALA for simulation-based estimation in cases where the dimension of the latent model is comparable to the number of observations. Its use with censored data for exceedance-based spatial extreme-value analysis allows bypassing high-dimensional numerical integration efficiently.

Hence, our assumed model structure coupled with a data augmentation approach can be efficiently exploited to fit complex models in relatively high dimensions to censored threshold exceedances.

In our spatiotemporal precipitation data application, we have opted for a two-step modeling approach of extreme episodes. Essentially, we first identify spatial extreme events, defined here as days with large spatially aggregated values at all locations, and then separately model their occurrences and intensities. More precisely, in the first step, we model the binary time series of occurrences (1's) or nonoccurrences (0's) of spatial extreme events through logistic regression, and in the second step, we model the precipitation intensities of extreme events using a spatial hierarchical gamma-gamma model. This two-step approach has the benefit of reducing the number of latent variables included in our Bayesian model fitted in the second step, speeding up computations. Temporal dependence may be incorporated through covariate or random effect modeling in the logistic regression. In future research, it would be interesting to further extend the latent process of our spatial hierarchical model to take the spatiotemporal dependence of successive extreme precipitation intensities into account.

ACKNOWLEDGMENTS

The authors would like to thank the Editor, Associate Editor, and a referee for valuable suggestions that have improved the manuscript. The data that support the findings of this study are openly available from the European Climate Assessment & Dataset project at <https://www.ecad.eu/>. This publication is based on work supported by the King Abdullah University of Science and Technology (KAUST) Office of Sponsored Research (OSR) under Award No. OSR-CRG2017-3434.

DATA AVAILABILITY STATEMENT

The data that support the findings of this study are openly available from the European Climate Assessment & Dataset project at <https://www.ecad.eu/>.

ORCID

Rishikesh Yadav  <https://orcid.org/0000-0003-3419-9356>

Raphaël Huser  <https://orcid.org/0000-0002-1228-2071>

Thomas Opitz  <https://orcid.org/0000-0002-5863-5020>

REFERENCES

- Andrieu, C., & Thoms, J. (2008). A tutorial on adaptive MCMC. *Statistics and Computing*, 18, 343–373.
- Arendarczyk, M., & Debicki, K. (2011). Asymptotics of supremum distribution of a gaussian process over a weibullian time. *Bernoulli*, 17(1), 194–210.
- Arneth, A., Denton, F., Agus, F., Elbehri, A., Erb, K., Osman Elasha, B., Rahimi, M., Rounsevell, M., Spence, A. and Valentini, R. (2019) Framing and context. In *Climate change and land: An IPCC special report on climate change, desertification, land degradation, sustainable land management, food security, and greenhouse gas fluxes in terrestrial ecosystems*, eds P. Shukla, J. Skea, E. C. Buendia, V. Masson-Delmotte, H.-O. Pörtner, D. Roberts, P. Zhai, R. Slade, S. Connors, R. van Diemen, M. Ferrat, E. Haughey, S. Luz, S. Neogi, M. Pathak, J. Petzold, J. P. Pereira, P. Vyas, E. Huntley, K. Kissick, M. Belkacemi and J. Malley. In press. https://www.ipcc.ch/site/assets/uploads/sites/4/2020/02/SPM_Updated-Jan20.pdf.
- Bacro, J.-N., Gaetan, C., Opitz, T., & Toulemonde, G. (2020). Hierarchical space-time modeling of asymptotically independent exceedances with an application to precipitation data. *Journal of the American Statistical Association*, 115, 555–569.
- Banerjee, S., Carlin, B. P., & Gelfand, A. E. (2014). *Hierarchical modeling and analysis for spatial data*. 2nd edition, CRC Press.
- Bopp, G. P., & Shaby, B. A. (2017). An exponential-gamma mixture model for extreme Santa Ana winds. *Environmetrics*, 28, e2476.
- Bortot, P., & Gaetan, C. (2014). A latent process model for temporal extremes. *Scandinavian Journal of Statistics*, 41(3), 606–621.
- Bortot, P., & Gaetan, C. (2016). Latent process modelling of threshold exceedances in hourly rainfall series. *Journal of Agricultural, Biological and Environmental Statistics*, 21(3), 531–547.
- Breiman, L. (1965). On some limit theorems similar to the arc-sin law. *Theory of Probability & Its Applications*, 10(2), 323–331.
- Carreau, J., & Bengio, Y. (2009). A hybrid Pareto model for asymmetric fat-tailed data: The univariate case. *Extremes*, 12(1), 53–76.
- Castro-Camilo, D., & Huser, R. (2020). Local likelihood estimation of complex tail dependence structures, applied to U.S. precipitation extremes. *Journal of the American Statistical Association*, 115, 1037–1054.
- Castro-Camilo, D., Huser, R., & Rue, H. (2019). A spliced Gamma-generalized Pareto model for short-term extreme wind speed probabilistic forecasting. *Journal of Agricultural, Biological and Environmental Statistics*, 24, 517–534.
- Cooley, D., Nychka, D., & Naveau, P. (2007). Bayesian spatial modeling of extreme precipitation return levels. *Journal of the American Statistical Association*, 102(479), 824–840.
- Cressie, N. A. C. (1993). *Statistics for spatial data*. Wiley Online Library.

- Davison, A. C., & Gholamrezaee, M. M. (2012). Geostatistics of extremes. *Proceedings of the Royal Society A: Mathematical, Physical & Engineering Sciences*, 468(2138), 581–608.
- Davison, A. C., & Huser, R. (2015). Statistics of extremes. *Annual Review of Statistics and Its Application*, 2, 203–235.
- Davison, A. C., Huser, R., & Thibaud, E. (2019). *Spatial extremes*. In A. E. Gelfand, M. Fuentes, J. A. Hoeting, & R. L. Smith (Eds.), *Handbook of Environmental and Ecological Statistics*. CRC Press.
- Davison, A. C., Padoan, S., & Ribatet, M. (2012). Statistical modelling of spatial extremes (with discussion). *Statistical Science*, 27(2), 161–186.
- Davison, A. C., & Smith, R. L. (1990). Models for exceedances over high thresholds (with discussion). *Journal of the Royal Statistical Society: Series B (Statistical Methodology)*, 52(3), 393–442.
- de Fondeville, R., & Davison, A. C. (2018). High-dimensional peaks-over-threshold inference. *Biometrika*, 105(3), 575–592.
- Dekkers, A. L., Einmahl, J. H., & De Haan, L. (1989). A moment estimator for the index of an extreme-value distribution. *The Annals of Statistics*, 17(4), 1833–1855.
- Eastoe, E. F., & Tawn, J. A. (2009). Modelling non-stationary extremes with application to surface level ozone. *Journal of the Royal Statistical Society: Series C (Applied Statistics)*, 58(1), 25–45.
- Fougères, A.-L., & Mercadier, C. (2012). Risk measures and multivariate extensions of Breiman's theorem. *Journal of Applied Probability*, 49(2), 364–384.
- Frigessi, A., Haug, O., & Rue, H. (2003). A dynamic mixture model for unsupervised tail estimation without threshold selection. *Extremes*, 5(3), 219–235.
- Gneiting, T., & Raftery, A. E. (2007). Strictly proper scoring rules, prediction, and estimation. *Journal of the American Statistical Association*, 102(477), 359–378.
- Huser, R., & Davison, A. C. (2014). Space-time modelling of extreme events. *Journal of the Royal Statistical Society: Series B (Statistical Methodology)*, 76(2), 439–461.
- Huser, R., Opitz, T., & Thibaud, E. (2017). Bridging asymptotic independence and dependence in spatial extremes using Gaussian scale mixtures. *Spatial Statistics*, 21, 166–186.
- Huser, R., & Wadsworth, J. L. (2019). Modeling spatial processes with unknown extremal dependence class. *Journal of the American Statistical Association*, 114, 434–444.
- Huser, R., & Wadsworth, J. L. (2020). Advances in statistical modeling of spatial extremes. *Wiley Interdisciplinary Reviews: Computational Statistics* To appear. e1537. <https://doi.org/10.1002/wics.1537>.
- Lerch, S., Thorarinsdottir, T. L., Ravazzolo, F., & Gneiting, T. (2017). Forecaster's dilemma: Extreme events and forecast evaluation. *Statistical Science*, 32(1), 106–127.
- Murawski, A., Zimmer, J., & Merz, B. (2016). High spatial and temporal organization of changes in precipitation over Germany for 1951–2006. *International Journal of Climatology*, 36, 2582–2597.
- Naveau, P., Huser, R., Ribereau, P., & Hannart, A. (2016). Modeling jointly low, moderate, and heavy rainfall intensities without a threshold selection. *Water Resources Research*, 52(4), 2753–2769.
- Opitz, T., Huser, R., Bakka, H., & Rue, H. (2018). INLA goes extreme: Bayesian tail regression for the estimation of high spatio-temporal quantiles. *Extremes*, 21(3), 441–462.
- Papastathopoulos, I., & Tawn, J. A. (2013). Extended generalised Pareto models for tail estimation. *Journal of Statistical Planning and Inference*, 143(1), 131–143.
- Power, S. B., & Delage, F. c. P. D. (2019). Setting and smashing extreme temperature records over the coming century. *Nature Climate Change*, 9, 529–534.
- Reiss, R.-D., & Thomas, M. (2007). *Statistical analysis of extreme values* (3rd ed.). Basel: Birkhäuser.
- Resnick, S. I. (1987). *Extreme values, regular variation and point processes*. Springer.
- Risser, M. D., & Wehner, M. F. (2017). Attributable human-induced changes in the likelihood and magnitude of the observed extreme precipitation during Hurricane Harvey. *Geophysical Research Letters*, 44(24), 12457–12464.
- Roberts, G. O., & Rosenthal, J. S. (1998). Optimal scaling of discrete approximations to Langevin diffusions. *Journal of the Royal Statistical Society: Series B (Statistical Methodology)*, 60(1), 255–268.
- Roberts, G. O., & Tweedie, R. L. (1996). Exponential convergence of Langevin distributions and their discrete approximations. *Bernoulli*, 2(4), 341–363.
- Rue, H., Riebler, A., Sørbye, S. H., Illian, J. B., Simpson, D. P., & Lindgren, F. K. (2017). Bayesian computing with INLA: A review. *Annual Review of Statistics and Its Application*, 4, 395–421.
- Scarrott, C., & MacDonald, A. (2012). A review of extreme value threshold estimation and uncertainty quantification. *REVSTAT*, 10(1), 33–60.
- Simpson, D. P., Rue, H., Riebler, A., Martins, T. G., & Sørbye, S. H. (2017). Penalising model component complexity: A principled, practical approach to constructing priors. *Statistical Science*, 32(1), 1–28.
- Stein, M. L. (2020a). Parametric models for distributions when interest is in extremes with an application to daily temperature. *Extremes* To appear. <https://doi.org/10.1007/s10687-020-00378-z>.
- Stein, M. L. (2020b). A parametric model for distributions with flexible behavior in both tails. *Environmetrics* To appear. e2658. <https://doi.org/10.1002/env.2658>.
- Vettori, S., Huser, R., & Genton, M. G. (2019). Bayesian modeling of air pollution extremes using nested multivariate max-stable processes. *Biometrics*, 75, 831–841.
- Vettori, S., Huser, R., Segers, J., & Genton, M. G. (2020). Bayesian model averaging over tree-based dependence structures for multivariate extremes. *Journal of Computational and Graphical Statistics*, 29, 174–190.

- Wadsworth, J. L., & Tawn, J. A. (2014). Efficient inference for spatial extreme value processes associated to log-Gaussian random functions. *Biometrika*, 101(1), 1–15.
- Witze, A. (2018). Why extreme rains are gaining strength as the climate warms. *Nature*, 563(7732), 458–460.

SUPPORTING INFORMATION

Additional supporting information may be found online in the Supporting Information section at the end of this article.

How to cite this article: Yadav R, Huser R, Opitz T. Spatial hierarchical modeling of threshold exceedances using rate mixtures. *Environmetrics*. 2021;32:e2662. <https://doi.org/10.1002/env.2662>